Overexpression of the microtubule-binding protein CLIP-170 induces a +TIP network superstructure consistent with a biomolecular condensate Yueh-Fu O. Wu<sup>1,2</sup>, Annamarie T. Bryant<sup>1,2</sup>, Nora T. Nelson<sup>1</sup>, Alexander G. Madey<sup>1</sup>, Gail F. Fernandes<sup>1</sup>, and Holly V. Goodson<sup>1,2,3\*</sup> <sup>1</sup>Department of Chemistry and Biochemistry, University of Notre Dame, Notre Dame, IN <sup>2</sup>Integrated Biomedical Sciences Graduate Program, University of Notre Dame, Notre Dame, IN <sup>3</sup>Department of Biological Sciences, University of Notre Dame, Notre Dame, IN \* Corresponding author E-mail: hgoodson@nd.edu (HVG) 

## **Abstract**

32

33

34

35

36

37

38

39

40

41

42

43

44

45

46

47

48

49

50

51

52

53

54

55

56

57

58

Proper regulation of microtubule (MT) dynamics is critical for cellular processes including cell division and intracellular transport. Plus-end tracking proteins (+TIPs) dynamically track growing MTs and play a key role in MT regulation. +TIPs participate in a complex web of intra- and inter- molecular interactions known as the +TIP network. Hypotheses addressing the purpose of +TIP:+TIP interactions include relieving +TIP autoinhibition and localizing MT regulators to growing MT ends. In addition, we have proposed that the web of +TIP:+TIP interactions has a physical purpose: creating a dynamic scaffold that constrains the structural fluctuations of the fragile MT tip and thus acts as a polymerization chaperone. Here we examine the possibility that this proposed scaffold is a biomolecular condensate (i.e., liquid droplet). Many animal +TIP network proteins are multivalent and have intrinsically disordered regions, features commonly found in biomolecular condensates. Moreover, previous studies have shown that overexpression of the +TIP CLIP-170 induces large "patch" structures containing CLIP-170 and other +TIPs; we hypothesized that these structures might be biomolecular condensates. To test this hypothesis, we used video microscopy, immunofluorescence staining, and Fluorescence Recovery After Photobleaching (FRAP). Our data show that the CLIP-170-induced patches have hallmarks indicative of a biomolecular condensate, one that contains +TIP proteins and excludes other known condensate markers. Moreover, bioinformatic studies demonstrate that the presence of intrinsically disordered regions is conserved in key +TIPs, implying that these regions are functionally significant. Together, these results indicate that the CLIP-170 induced patches in cells are phase-separated liquid condensates and raise the possibility that the endogenous +TIP network might form a liquid droplet at MT ends or other +TIP locations.

## Introduction

59

60

61

62

63

64

65

66

67

68

69

70

71

72

7374

75

76

77

78

79

80

81

82

83

84

8586

87

88

Microtubules (MTs) compose one of the three major filament networks of the eukaryotic cytoskeleton, and they are required for basic cellular functions such as cell polarity, cell division, and intracellular transport. Dysfunction of the MT cytoskeleton can lead to serious neurodegenerative diseases including tauopathies and Parkinson's disease, and compounds that target MTs are significant as chemotherapy agents, fungicides, and herbicides (1, 2). Microtubules display a surprising behavior known as dynamic instability, which describes the approximately random alteration between phases of slow growth (polymerization) and rapid shrinkage (depolymerization). This behavior is regulated by MT binding proteins and is central to MT function because it enables MTs to explore space to respond rapidly to internal and external signals and find organelles to be transported (reviewed by (2)). The most conserved MT binding proteins (and by implication the most important) are a set of mutually interacting proteins that dynamically track growing MT ends and are collectively known as microtubule plus-end tracking proteins (+TIPs). +TIPs form an interaction network created by many weak, multivalent links (both intra- and intermolecular) between MTs and +TIPs (2, 3). While many +TIPs and their MT regulatory roles have been identified, it is not yet fully understood why so many +TIPs bind to other +TIPs. One favored explanation is that the interactions of the +TIP network create regulatory pathways by relieving the autoinhibition feature present in many +TIP proteins (Fig 1A). Another explanation is that +TIP:+TIP interactions serve to localize and deliver proteins in a spatiotemporal manner (e.g. localizing +TIPs to the MT ends, and facilitating the surfing of proteins to cell edge) (reviewed in (3)). Fig 1. Conceptual models of the +TIP network. (A) In the regulation-focused model of the +TIP network, interactions between +TIPs function primarily to activate autoinhibited +TIP proteins and/or enable +TIPs to localize to the plus end. (B) In a more physical model of the +TIP network, interactions between +TIP

proteins form a cross-linked, dynamic scaffold that supports and stabilizes the fluctuating MT tips by promoting lateral binding of protofilaments (4). This figure was created with BioRender (5). While these explanations for the existence of the +TIP network are logical, some aspects of +TIP behavior seem inconsistent with either idea, suggesting that this set of explanations is not complete. For example, deletion of evolutionarily conserved +TIPs often has surprisingly little effect on MT dynamics and/or cell survival (S1 Table), which is especially surprising if the localization and/or activity of some conserved +TIPs depend on others. In addition, while individual +TIPs can function independently in regulating MT dynamics, evidence from several labs also suggests that groups of +TIPs work synergistically to promote MT polymerization (4, 6, 7). Such synergy seems inconsistent

with linear regulatory and/or localization pathways, which would predict epistasis or at

most additive effects. These observations led us to suggest in earlier work that the

interactions of the +TIP network have an important additional function, which is to

create a superstructure that promotes MT assembly by constraining the structural

fluctuations of the MT tip (Fig 1B) (4).

The work in this paper focuses on the +TIP CLIP-170, which was the first characterized +TIP (8). Previous studies have found that CLIP-170 promotes interactions between organelles and MTs (8-10) and regulates MT dynamics (11). CLIP-170 has also been implicated in actin-MT crosstalk (e.g., (12-14)). Similar to other +TIPs, CLIP-170 has multiple conserved binding sites that mediate interactions with MTs and/or other +TIPs (15, 16). Structurally, CLIP-170 contains three major domains. The N-terminal head domain is composed of two CAP-Gly subdomains and three serine-rich regions, all of which contribute to MT binding (15). The coiled-coil region mediates CLIP-170 dimerization (17) and contains a FEED domain, which forms a complex with formin and actin to promote actin polymerization (12). The C-terminal domain contains two zinc-knuckle motifs (9, 17, 18): the first of these mediates CLIP-170:CLIP-170 interactions involved in autoinhibition, while the second mediates an interaction with the dynein-associated dynactin complex (19, 20).

Overexpression of CLIP-170 causes formation of so-called "patches" (9, 19). The physical identity of these patches was puzzling to the researchers performing early work on CLIP-170, who initially assumed that the patches were membranous organelles of some kind but were not able to colocalize membrane markers to them. These early efforts showed that CLIP-170 could recruit other proteins more recently recognized as +TIPs (specifically EB1 and dynactin complex) into the patches (19). These characteristics and others described below led us to speculate that the patches might correspond to biomolecular condensates. The goal of the work described in this paper is to investigate this possibility and consider its potential implications in terms of the form and function of the +TIP network under normal physiological conditions. Biomolecular condensates (aka liquid droplets, coacervates, membraneless organelles) are dynamic structures that spontaneously form when interactions between groups of weakly-binding biopolymers (protein and sometimes RNA or DNA) cause them to phaseseparate from surrounding cytoplasm or nucleoplasm (21-24). Cytosolic examples include P-bodies, which regulate mRNA turnover (25, 26), Wnt signalosomes, which help to transduce Wnt signaling (27-29), and the pericentriolar material/matrix, which regulates MT nucleation at the centrosome (30, 31). In the nucleus, Cajal bodies regulate RNA-related metabolism (32), and PML bodies regulate nuclear functions (33). While these biomolecular condensates are associated with functions that promote cell survival, not all are positive: condensates of the MT-associated protein Tau corelate with the progression of Alzheimer's disease (34-36). The process in which proteins/nucleic acids self-assemble into a condensate is called liquid-liquid phase separation (LLPS). This liquid-liquid demixing process becomes observable when the proteins/nucleic acids reach a critical concentration (21-24). Biomolecules identified as forming condensates generally contain intrinsically disordered regions (IDRs) and multivalent binding regions that mediate weak interactions. These sequence features generate the driving forces for condensate formation (21-24). Physical factors such as temperature and pH can affect the condensation or dissolution of LLPS as well (21-24).

120

121

122

123

124

125

126

127

128

129

130

131

132

133

134

135

136

137

138

139

140

141

142

143

144

145

146

147

148

149

150

While many condensates are now well-recognized (21, 24), there are relatively few examples of mechanistically defined functions for condensate formation. Proposed functions include concentrating reactive molecules locally to promote cellular reactions (e.g., promoting actin nucleation (37)), serving as a storage depot (e.g., P-granules (25)), and providing mechanical forces to generate local viscoelasticity, which can be important to resist the deformation of cellular structures (e.g. condensate formation at the centrosome (38)). Even though the functions and localizations of these condensates are varied, some attributes are shared between them. Common hallmarks that are thought to identify a biomolecular condensate include a) elastic deformability, b) the ability to undergo fusion and fission, c) selectivity (i.e., inclusion of certain biomolecules and the exclusion of others), and d) rapid exchange of proteins between the droplets and the cytoplasm (21-23, 39).Here, we use live-cell imaging, photobleaching, and immunofluorescence to show that the "patches" previously observed as being induced upon CLIP-170 overexpression have the four hallmarks of liquid-liquid condensates, leading us to conclude that the patches are biomolecular condensates. We also evaluated the sequence properties of CLIP-170 and other +TIPs for the presence of sequence characteristics associated with condensate formation. We show that many +TIPs both are multivalent and contain IDRs, and that for key +TIPs these sequence features are conserved across large spans of evolution, suggesting that they are functionally significant. These data are consistent with our previous proposal that the +TIP network forms a physical superstructure and lead us to speculate that this superstructure is (in at least some circumstances or locations) a biomolecular condensate that coats the MT tip to support and promote MT assembly.

152

153

154

155

156

157

158

159160

161

162

163

164

165

166167

168

169

170

171

172

173

174

175

176

177

178

179

180

# **Materials and Methods:**

183	Cell lines and cell culture		
184	NIH3T3 cells (a gift of Dr. Reginal Hill) were grown in Dulbecco's Modified Eagle Medium		
185	(DMEM, Sigma) plus 2% glutamine (BioWhittaker) and 10% bovine calf serum (VWR).		
186	Cos-7 cells (a gift of Dr. Kevin Vaughan) were grown in DMEM plus 1% glutamine and		
187	10% fetal bovine serum (Sigma). Cells were incubated under standard cell culture		
188	conditions (37°C and 5% CO <sub>2</sub> ).		
189			
190	DNA constructs		
191	CLIP-170 constructs utilize the version of CLIP-170 used in the original Kreis lab		
192	publication (8), now described in accession AAA35693. CLIP-170 plasmids with		
193	expressed transgenes under control of the CMV promoter have been described		
194	previously: WT CLIP-170 in pSG5 vector (pSG5-myc-CLIP-170) (40), and the N-terminal		
195	EGFP-conjugated WT CLIP-170 in pCB6 vector (pCB6-GFP-CLIP-170, "GFP-CLIP-170" here		
196	after) (41). mEmerald-CLIP170-N-18, hereafter called N-18, was a gift from Michael		
197	Davidson (Addgene plasmid # 54044). N-18 has an mEmerald tag at the C-terminus. The		
198	N-18 GSSG construct lacks the mEmerald but has extra 4 amino acid GSSG tag at the C-		
199	terminus of CLIP-170, while the N-18 ETF construct has a stop codon after the native C-		
200	terminus (ETF) of CLIP-170.		
201			
202	Antibodies & lipid dyes		
203	The CLIP-170 antibodies used in this study were either a rabbit polyclonal raised against		
204	Xenopus CLIP-170 (this manuscript) or the mixture of mouse monoclonal antibodies		
205	4D3/2D6 (8, 42), with the exception of the GalT colocalization experiment, which		
206	utilized the rabbit polyclonal $\alpha55$ raised against human CLIP-170 (8). p150 was		
207	recognized by rabbit polyclonal anti-p150 $^{ ext{Glued}}$ , which was a gift from K. Vaughan and R.		
208	Vallee. EEA1 was recognized by rabbit polyclonal anti-EEA1 (43). The monoclonal		
209	antibody against GalT was a gift to Dr. Thomas Kris from Dr. T. Suganuma (44). Other		
210	primary antibodies were obtained from commercial sources: hnRNPA1 - mouse		
211	hnRNPA1 monoclonal antibody 4B10 (Invitrogen, MA5-24774), YB1 - rabbit YB1		
212	polyclonal antibody D299 (Cell Signaling, 4202S), Staufen1 - rabbit polyclonal antibody		

213	(Bios antibodies, bs-9877R), CLASP1 - rat monoclonal antibody (Absea, KT66), CLASP2 -		
214	rat monoclonal antibody (Absea, KT69), mDia2 - rabbit DIAPH3 polyclonal antibody		
215	(Proteintech, 14342-1-AP), EB1 - mouse monoclonal antibody (Transduction		
216	Laboratories, now BD-Transduction, 610534), LIS-1 - mouse monoclonal antibody H-7		
217	(Santa Cruz, sc-374586), and tubulin – mouse monoclonal antibody 1A2 (Sigma, T9028).		
218	All labeled secondary antibodies were obtained from Invitrogen. Generic RNA was		
219	stained with SYTO™ RNASelect™ Green Fluorescent Cell Stain (Thermo Fisher, S32703).		
220	Rhodamine DHPE (Thermo Fisher, L-1392), Dil (Invitrogen), and RhPE (Molecular Probe		
221	were used as generic membrane labels. LysoTracker (Molecular Probes, DND-99) and		
222	MitoTracker Red CMXRos (Cell Signaling) were used to stain lysosomes and		
223	mitochondria, respectively. For all membrane staining experiments, cells were stained		
224	according to manufacturer protocols, and then moved into imaging medium for		
225	imaging.		
226			
227	Transient transfections		
228	For fixed cell images, cells were grown on 10 mm <sup>2</sup> glass coverslips (Knittel Glaser). For		
229	live cell imaging, cells were grown on 35 mm dishes with 10 mm glass bottom coverslips		
230	(P35G-1.5-10-C, MatTek) or 8-well glass-bottom chambers (Eppendorf). Cells were		
231	transiently transfected by Lipofectamine 3000 (Invitrogen, L3000008) with 5 $\mu g$ of		
232	indicated construct DNA per reaction when cells reached 70-80% confluence. For		
233	consistency, cells were incubated for 24 hr post-transfection before performing live		
234	imaging, FRAP, and immunofluorescence assays unless otherwise indicated.		
235			
236	Heat shock and drug treatment		
237	Cells that underwent heat shock or drug treatments are indicated in their figure legends.		
238	To induce stress granules, NIH3T3 cells were incubated at 42°C or treated with 0.5 mM		
239	NaAsO <sub>2</sub> for one hour before fixation as indicated in the figure legend. To study the		
240	relationship between CLIP-170-induced patches and tubulin/MTs, NIH3T3 cells were		
241	incubated with 5 $\mu M$ Nocodazole for 16 hr or 1 hr before fixation as indicated in the		
242	figure legend. For consistency, all cells were incubated for 24 hr post-transfection		
243	before fixation unless otherwise indicated, regardless of possible heat shock or drug		
244	treatment.		

# Immunofluorescence

245

246247

248

249

250

251

252

253

254

255

256

257

258

259

260

261

262

263

264

265

266

267

268

269

270

As indicated in the figure legends, cells were fixed by methanol or 3% paraformaldehyde (PFA) before staining with the antibodies described above. For the methanol fixation, cells were fixed in -20°C methanol for 4 min and washed three times with PBS before treatment with primary antibodies. For the PFA fixation, cells were fixed in 3% PFA for 20 min, washed once with PBS, quenched with a wash of 30 mM ammonium chloride in PBS, and washed once again in PBS. Cells were then permeabilized with 0.1% Triton-X-100 for 4 min and washed with PBS again before treating with primary antibodies. Each washing step was 5 min. Cells were incubated with the primary antibody for 20 min, washed three times with PBS, incubated with the indicated fluorophore-conjugated secondary antibodies for 20 min, and washed three times with PBS. Cells were mounted on slides in Mowiol 4-88 mounting medium (Sigma 475904-M). Unless otherwise indicated, images were acquired with a 100x objective (1.4 N.A.) and a 1.5× optivar on a TE2000 inverted microscope (Nikon) with a Hamamatsu CMOS camera controlled by NIS-Elements BR 413.04 64-bit software (Nikon). Alternatively, microscopy was performed on a DeltaVision Deconvolution Microscope (GE Healthcare) with a 60x 1.42 N.A. objective connected to a Photometrics Coolsnap hq2 monochrome camera controlled by Resolve3D – SoftWoRx 7.0.0 software (GE Healthcare). Images were processed using Fiji (National Institutes of Health, https://imagej.net/Fiji) (45). For the EEA1 and GalT immunofluorescence experiments in Supplementary Information, cells were imaged using a 40x 1.4NA PlanApo objective on a Zeiss inverted microscope (TV135); images were recorded with a cooled CCD camera (Photometrics CH250, Tuscon AZ) driven by IPLab-Spectrum software (Scanalytics, Fairfax VA), and processed by Photoshop (Adobe). Because CLIP-170 patches can be very bright, negative controls with one primary and two secondary antibodies were routinely performed to assess levels of signal created by bleed through and/or antibody cross-reactivity.

271272

273

274275

276

# Live imaging and Fluorescence Recovery After Photobleaching (FRAP)

Live imaging experiments were performed either with an A1R-MP Laser Scanning Confocal Microscope or with DeltaVision as indicated. In both systems, cells were

incubated at  $37^{\circ}$ C with 0.5% CO<sub>2</sub> within an environmental chamber. DMEM culture media lacking phenol red (Sigma, 51449C) plus 2% glutamine and 10% bovine calf serum (VWR) was used during live imaging processes.

For the FRAP measurements, FRAP experiments were performed on the A1R-MP Laser Scanning Confocal Microscope (Nikon) using a 100x 1.49NA oil immersion objective, which was driven by Nikon NIS-Elements software and was equipped with PMT detectors. Condensates were bleached with a solid state laser (Coherent) with a 488 nm, 100% laser intensity for 200 ms. Time-lapse images were acquired before and after photobleaching at two frames per sec for 9 loops and 82 loops, respectively. We set the bleach regions as a 1  $\mu$ m diameter circle, though the region that was actually affected by the bleaching was ~1.5-2  $\mu$ m in diameter.

Images were processed using FIJI to measure the intensity of the regions of interest (FRAP region, background region, and the reference region) before and after photobleaching. The selection of regions of interest and FRAP analysis were performed following the guide of the protocol of the Aravin lab and EMBL (46). Briefly, we measured the intensity of three different regions to assess photobleaching: (1) BL: the region that was bleached by the laser, (2) BG: a region outside of the cell, used to measure the level of background signal, and (3) REF: a region inside of the cell but outside the bleached region, used to assess the decay of signal from imaging-associated photobleaching. After determining the intensities of the three regions over time, we subtracted the background signal (BG) from the BL and REF regions and normalized the fluorescence decay by dividing BL by REF to get the normalized intensity over time I(t):

 $I(t) = \frac{BL-BG}{REF-BG}$ . Next, to calculate the fraction of fluorescence recovery after

302 photobleaching, we divided the intensity after bleaching by the mean intensity before

bleaching to get:  $FRAP(t) = \frac{I(t, post-bleaching)}{I(mean intensity of pre-bleaching)}$ . Plotting FRAP(t) over

time gave an intensity curve such as that shown in (Fig 6B). Finally, we used

MATLAB(R2019a) to fit the intensity curve with the equation FRAP(t) = a \*

 $306 \quad (1 - e^{-bt}) + c$ , where a is the slowly recovering fraction; b is recovery rate constant; c

307 is the rapidly diffusing fraction (46-49). The fraction of mobile protein = a+c, and the 308 fraction of immobile protein = 1-(a+c). The halftime of recovery  $(t_{1/2}) = \ln 2/b$ . 309 **Bioinformatics** 310 311 Identification of +TIPs in other organisms 312 A range of nine model organisms (from plants to humans) was chosen to assess the 313 conservation of the presence of intrinsically disordered regions (IDRs) in a set of well-314 recognized +TIP network proteins. The selected organisms are: Homo sapiens (taxid:9606), Mus musculus (taxid:10090), Xenopus laevis (taxid:8355), Danio rerio 315 316 (taxid:7955), Drosophila melanogaster (taxid:7227), Saccharomyces cerevisiae 317 (taxid:4932), Schizosaccharomyces pombe (taxid:4896), Dictyostelium discoideum AX4 318 (taxid:352472), and Arabidopsis thaliana (taxid:3702). 319 320 To identify core +TIPs (or other relevant proteins) in these organisms, we performed a 321 BLASTp (or when necessary, a PSI-BLAST) search in the NCBI RefSeq database using the 322 following representative human sequences as probes: CLIP-170 (AAA35693.1), EB1 323 (NP 0364571), MAP215 (NP 0010089381), CLASP2 (NP 0013525571), CLASP1 324 (NP\_0560971), p150 (NP\_0040732), LIS-1 (NP\_0004211), APC (NP\_0013418251), and 325 mDia2 (NP 0010359821). In many cases (e.g., EB1), identification of unambiguous 326 homologs was straightforward from examination of the e-values and alignments; in 327 cases where gene duplications had occurred, we chose the gene with the strongest 328 (lowest) e-value for further analysis. In cases of alternative splicing, we chose the 329 longest of the curated transcripts for further analysis, except for CLIP-170 and CLASP 330 homologs, where we chose the form that best matched the domain structure of the 331 human protein used as the probe. Note that CLIP-170 homologs were not identified in 332 Dictyostelium or Arabidopsis. 333 334 **Bioinformatic tools used** 335 IDR prediction: We focused our efforts on three IDR predictors, which were used with 336 default parameters unless otherwise indicated: 1) "ESpritz version 1.3" (50) 337 (http://old.protein.bio.unipd.it/espritz/), used with prediction type as X-Ray and 338 decision threshold as 5% false positive rate (5% FPR; chosen because the default setting

["Best Sw" – a weighted score rewarding prediction of IDRs] tends to overestimate IDRs); 2) "Interpro" (EMBL, https://www.ebi.ac.uk/interpro/), which provides as part of its standard analysis disorder predictions from the MobiDB-lite database (51)); and 3) "IUPred2", used with "short disordered" setting, as obtained from the IUPred2A server (https://iupred2a.elte.hu/) (52, 53). We chose these three out of the wide array of possible IDR predictors because they are widely-used (54), and in our preliminary analyses they rarely generated spurious reports of coiled-coil regions as IDRs, unlike some others, e.g., PONDR. In Fig 7, we present the results of all three methods for human CLIP-170; for other analyses, we simplified the display by showing only the results from the first two predictors because the results from Espritz and IUPred2 were similar. The likelihoods of intrinsic disorder as a function of amino acid position as produced by ESpritz and IUPred2 were plotted by MATLAB(R2019a). For MobiDB-lite predictions, we manually listed all predicted IDRs as obtained from Interpro. Then, we plotted the list of IDRs with the MATLAB(R2019a) "patch" function. Other analyses: Sets of orthologous protein sequences were aligned by ClustalW (55) or alternatively PASTA (56). For most of the domain structure predictions, we used a hmmscan Pfam search with e-value 0.1 at HMMER (https://www.ebi.ac.uk/Tools/hmmer/search/phmmer) (57) (S8-S11 Figs). The only exception was CLIP-170 and its homologs. To map the domain structure of CLIP-170 homologs, we extracted from the NCBI protein information page the location of CAP-Gly domains, serine-rich regions, and zinc-knuckle motifs. Then, we aligned the human CLIP-170 FEED domain (VEEESITKGDLE) (12) to the representative sequences of other organisms to identify the FEED domain. Lastly, we combined all the domain information and plotted the protein sequence with "IBS Version 1.0" (http://ibs.biocuckoo.org/online.php). To predict coiled-coil regions, we used the "COILS" predictor (https://embnet.vital-it.ch/software/COILS form.html) (58) with default settings.

339

340

341

342

343

344

345

346

347

348

349

350

351

352

353354

355

356

357

358

359

360

361

362

363

364

365

366

367

## **Results:**

370

371

372

373

374

375

376

377

378

379

380381

382

383

384385

386

387

388

389

390

391

392

393

394

395

396

397

398

399

400

The overall goals of this study were to test whether the so-called "patches" induced by CLIP-170 overexpression (9, 19) are biomolecular condensates and, if so, to then consider the implications of this observation for the structure and function of the +TIP network under normal physiological conditions. Although it would be ideal to examine the endogenous +TIP network directly, the "comets" at the ends of MT plus ends are both dynamic and small (near the diffraction limit of visible light), making it technically difficult to determine clearly whether they have condensate properties. Thus, although CLIP-170 patches are themselves overexpression artifacts, we hypothesized that they might reflect some properties of physiological +TIP networks and so used them as a tool to gain insight into these properties. As evidence that this approach can be fruitful, in previous work we successfully used this same logic to identify the +TIPs EB1 and dynactin complex as CLIP-170-interacting proteins and showed that the interactions were mediated by different regions of the CLIP-170 protein (19). As noted above, four properties common to biomolecular condensates are 1) elastic deformability, 2) the ability to undergo fusion and fission, 3) selectivity: droplets include certain members but exclude others, and 4) rapid exchange of proteins between the droplets and the cytoplasm (21-23, 39). Thus, we examined the CLIP-170-induced patches for each of these characteristics in turn. In addition, proteins included in droplets generally have the following structural characteristics that are important for droplet formation: they have multiple sites for binding other droplet members (i.e., they are multivalent), and they contain intrinsically disordered regions (IDRs). Accordingly, we also examined CLIP-170 and other +TIPs for these characteristics. CLIP-170 induces formation of so-called "patches" upon overexpression. As shown previously, when CLIP-170 is expressed at low levels, it labels MT plus ends ((8, 41, 59); see also Movies 1-2), but at higher levels it causes increasing formation of patches and MT bundles (Fig 2B, (9, 19); see also Movies 3-4). This phenomenon is seen in a range of cell types, including HeLa (9, 19), Cos-7 ((19), Fig 2B), and NIH3T3 (Fig 2B).

Fig 2. CLIP-170 patches do not colocalize with membrane markers. (A) Domain structures of the CLIP-170 constructs used in this study. (B) NIH3T3 or Cos-7 cells (as indicated) were transfected for 24 hr to overexpress GFP-CLIP-170, fixed with PFA, and observed by widefield fluorescence microscopy. Arrows point out examples of CLIP-170 patches as observed in cells at varied expression levels as indicated. The contrast of each image in a given row was adjusted to the same levels, except for high-level expression, where the main image was adjusted to allow the visualization of large and bright patch structures, and an inset provides a version normalized to match the rest of the row. (C) As an example of the failure of membrane markers to colocalize with patches, NIH3T3 cells were transfected with GFP-CLIP-170 for 24 hours. Rhodamine-DHPE or Rhodamine-PE was used as a generic membrane label to stain lipid membranes. Live cells were observed by widefield fluorescence microscopy. See S2 Fig for colocalizations with additional membrane markers. Scale bar: 10 μm This patch formation requires an intact second zinc knuckle (19). In addition, we observed that the ability of CLIP-170 constructs to induce patches requires a free CLIP-170 C-terminus: either a GFP or a short tag of 4 amino acids at the C-terminus prevents patch formation (S1 Fig, N-18 and N-18 GSSG). Strikingly, the ability of CLIP-170 to induce patch formation can be rescued by insertion of a stop codon before the Cterminal tag, thus reconstituting the original C-terminus (S1 Fig N-18 ETF). These observations provide evidence that the ability of CLIP-170 to induce patches requires specific sequences and is thus not a generic effect of CLIP-170 overexpression. The CLIP-170-induced patches do not colocalize with membranes To test whether the patches are membraneless, we first examined the patches for colocalization with various specific membrane markers, including MitoTracker, LysoTracker, ER tracker, GalT (labels Golgi), and EEA1 (labels endosomes). None of these, with the possible exception of EEA1, showed any significant colocalization with the CLIP-170 patches (S2 Fig). One problem with using specific makers to test for membrane presence is that cells contain many different membrane-bound compartments, and so negative results are not definitive: we might simply have failed to test for the appropriate compartment. Therefore, we tested for the presence of membranes more generally by looking for

401

402

403

404

405

406

407

408

409

410

411

412413

414

415

416

417

418

419

420

421422

423

424

425

426

427

428

429

430

431

colocalization with the nonspecific membrane dyes Rhodamine-DHPE and Rhodamine-PE. We observed no obvious colocalization with either dye (Fig 2C). These results are consistent with the hypothesis that the CLIP-170-induced patches are membraneless biomolecular condensates. Therefore, we proceeded to test for the presence of other characteristics of biomolecular condensates. CLIP-170 patches can elastically deform and undergo fusion and fission As discussed above, another characteristic of biomolecular condensates is that they can undergo elastic deformations, fission, and fusion. To test whether CLIP-170 patches exhibit these activities, we overexpressed GFP-CLIP-170 in NIH3T3 cells and used live cell fluorescence microscopy to monitor the GFP-CLIP-170 behavior over time. As shown in Fig 3 and Movie 3, CLIP-170 patches do indeed display fusion events (magenta arrow) and fission events (red box). In addition, it is common to see CLIP-170-labeled +TIP comets travel through and deform the CLIP-170 patches (Fig 3 and Movies 3-4). This observation indicates that the CLIP-170 patches interact with the +TIP network and suggests that these two structures may share some properties with each other. Taken together, these results indicate that the CLIP-170 patches have the elastic deformability, fusion, and fission properties expected of a biomolecular condensate. Fig 3. Dynamic behaviors of CLIP-170 patches in vivo. NIH3T3 cells were transfected to overexpress GFP-CLIP-170, and the behavior of GFP-CLIP-170 in vivo was recorded by confocal microscopy after 24-27 hr of transfection. Red box: An example of an apparent elastic deformation of a patch, following by fission (blow-up of this region is shown below). Arrows indicate examples of patch fusion (magenta), a photobleached site (green, relevant to discussions below), and a typical comet-shaped +TIP localization on a MT tip (yellow). CLIP-170 patches selectively recruit some cytoskeletal proteins but exclude members of other biomolecular condensates The next biomolecular condensate property we tested was selectivity: do CLIP-170 patches selectively recruit some proteins and exclude others? To address this question, we used immunofluorescence staining to test various molecules for patch colocalization.

433

434

435

436

437

438

439

440

441

442

443

444

445

446

447

448

449

450

451452

453

454

455

456

457

458459

460

461

462

The two groups of markers we tested were: (1) members of the +TIP network and (2) proteins included in established cytosolic liquid droplets (Table 1).

Table 1. List of molecules we have tested for co-localization with CLIP-170 patches

Protein	Included/excluded	Protein marker of
EB1	Included	+TIPs
LIS-1	Included	+TIPs
APC	NSAI	+TIPs and Wnt signaling
CLASP1	Included	+TIPs
CLASP2	Included	+TIPs and Golgi
MAP215	NSAI	+TIPs
p150	Included	+TIPs and Dynactin
mDia2	Included	Formin
RNA	Excluded	RNP granules
YB1	Excluded	Stress granules and P-bodies
hnRNPA1	Excluded	RNP granules
Staufen1	Excluded	RNP granules
Tubulin	Included	

Experiments were conducted in NIH3T3 cells. NSAI indicates "No Suitable Antibody Identified" due to lack of suitable antibodies. See Fig 4 and S3 Fig for images of the colocalizations summarized above.

As expected from previous work (9, 19), the +TIPs EB1 and p150 dynactin were observed to be recruited to the CLIP-170 patches (Fig 4, Table 1). In addition, we found that the patches recruit the +TIPs LIS1, CLASP1, CLASP2, as well as mDia2, an actin nucleator that binds EB1 (60) and so might be described as a peripheral part of the +TIP network (Fig 4, S3 Fig, and Table 1). However, antibodies against at least one other protein that has been described as MT binding (Staufen1) did not colocalize with CLIP-170 patches (S3 Fig, Table 1).

**Fig 4. CLIP-170 patches have selective properties.** NIH3T3 cells were transfected with full-length CLIP-170 for 24 hr before fixation and staining as indicated. For the EB1, p150, and YB1 labeling, cells were fixed with methanol; for LIS1 and mDia2, cells were fixed with PFA. The contrast of all images in a given row

was set to the same levels. These data show that EB1, p150, LIS-1, and mDia2 were included in the CLIP-170 patches; YB1 is an example of a molecule that was excluded from the patches. See S3 Fig for images of colocalizations with other molecules, and see Table 1 for a summarized list. Scale bar:  $10 \, \mu m$ .

To test for possible overlap between the CLIP-170 patches and other biomolecular condensates, we checked markers of RNP granules, P-bodies, and stress granules for colocalization to the patches. None were included in the CLIP-170 patches under our normal culture conditions (Fig 4, S3 Fig, and Table 1). Because stress granules are typically visible only under stress, we also tested colocalization with the stress granule protein YB1 after 42°C heat shock or 0.5 mM NaAsO<sub>2</sub> (a classical stress inducer for YB1 containing stress granules (61)); we also examined Staufen1 after 42°C heat shock. The heat shock did induce the formation of structures containing these proteins, but they did not colocalize with the CLIP-170 patches (Fig 4, S3 Fig, and Table 1).

One question not addressed above is whether the patches colocalize with MTs and/or tubulin. We observed that colocalization of the patches with MTs was variable. Staining in methanol-fixed cells under normal cell culture conditions typically revealed a tangle of MTs colocalized with the patches (Fig 5B, top row, see also (19)). However, in PFA-fixed cells, the tubulin staining was sometimes limited to the outside of the patch (S4 Fig, see also (9)).

Figure 5. MTs are not required for CLIP-170 patch formation and maintenance. (A) Experimental design diagram. (B) NIH3T3 cells were transfected with full-length CLIP-170, and cells were treated with 5  $\mu$ M nocodazole (Noc) after 8 hr (Set 1) or 23 hr (Set 2) transfection at 37 °C. Cells were fixed with methanol after 24 hr transfection, probed with antibodies against molecules of interest (as indicated), and observed by widefield fluorescence microscopy. After the nocodazole treatment, tubulin and EB1 colocalized with CLIP-170 patches, while YB1 did not colocalize with the patches. Each image was normalized separately to allow the visualization of the different staining and patches. Scale bar: 10  $\mu$ m.

The colocalization between patches, MT-binding proteins (Fig 4 and S3 Fig) and MTs (Fig 5B, top row and S4 Fig) as discussed above suggests a functional relationship with MTs. Therefore, we examined the effect of nocodazole on colocalization between patches

514 and anti-tubulin antibodies. In setting up this experiment, we had two considerations. 515 First, we wanted to see whether the patches are maintained in nocodazole-treated cells. 516 Second, we wanted to see if patch formation requires MTs. Therefore, we transfected 517 cells grown on coverslips with CLIP-170 and performed nocodazole treatments at two 518 timepoints, as diagrammed in Fig 5A. 519 520 For the first time point (Fig 5A, Set 1), we treated some of the coverslips with 521 nocodazole after eight hours of transfection, which is early in the transfection process 522 and thus before significant expression of plasmid-based CLIP-170 or patch formation 523 would be expected. We then continued to incubate these coverslips in nocodazole and 524 fixed and imaged them at the end of the experiment, i.e., after 24 hours of transfection. 525 For the second time point (Fig 5A, Set 2), we treated some coverslips with nocodazole 526 after 23 hours of transfection, a time when patches are prominent in many transfected 527 cells. We then fixed and imaged these coverslips at the same time as the coverslips from 528 the first time point, i.e., after the same 24 hours of transfection. 529 530 In this experiment (results provided in Fig 5B), we observed that MTs had disassembled 531 in both sets of nocodazole-treated cells, as expected. Significantly, we also found that 532 patches were observed in both sets of nocodazole-treated cells. Consistent with earlier 533 results showing that EB1 is recruited to the CLIP-170 patches (Fig 4 and (19)), the CLIP-534 170 patches in nocodazole-treated cells also contained EB1. In addition, the stress-535 granule marker YB1 was still excluded from patches in nocodazole-treated cells, even 536 though nocodazole induced the formation of stress granules (Fig 5B). 537 538 The observation that patches are observed in both sets of nocodazole-treated coverslips 539 (Fig 5B, Set 1 and Set 2) indicates that MTs are not required for patch maintenance. 540 However, we cannot rule out the possibility that small numbers of nocodazole-stable 541 MTs are sufficient for patch maintenance. The observation that patches were observed 542 at the end of the experiment in Set 1 initially suggested that MTs are not needed for 543 patch formation, since (as noted above), we expected that no cells would have patches 544 when these cells were treated with nocodazole (i.e., after eight hours of transfection). 545 However, to our surprise, we found that some transfected cells did have patches when

fixed at this 8 hr time point (Fig S5). Therefore, whether patch formation requires MTs remains a question for further study. Regardless, in both sets of nocodazole-treated cells, tubulin was clearly recruited to the patches, as evidenced by the bright tubulin staining (Fig 5).

Taken together, these data demonstrate that CLIP-170 patches selectively include a specific set of +TIP network proteins as well as tubulin (at least in nocodazole), while excluding members of several other known biomolecular condensates. This selective property is again consistent with the idea that the patches are biomolecular condensates. Furthermore, the observation that known condensate markers are excluded from the patches suggests that they are novel biomolecular condensates.

#### CLIP-170 in the patches exchanges rapidly within the cytoplasm

Another expected characteristic of a biomolecular condensate is the rapid molecular exchange of molecules between the condensate and the cytoplasm. A technique commonly used to assess such exchange is Fluorescence Recovery After Photobleaching (FRAP). We performed FRAP assays on the CLIP-170 patches and observed that the fluorescence intensity of the photobleached spots recovered quickly (half time of recovery ( $t_{1/2}$ ) =  $8.59 \pm 4.05$  sec) and to a large degree ( $0.66 \pm 0.21$  mobile fraction) (see example in Fig 6). This rate and degree of recovery of CLIP-170 patches is consistent with those reported for other biomolecular condensates (62).

Fig 6. FRAP analysis of the dynamics of CLIP-170 patches. (A) Example of a partially photobleached CLIP-170 patch in an NIH3T3 cell. (B) The time course plot for the FRAP spot in (A). This panel is one example representing the fluorescence recovery of one bleaching site in one CLIP-170 patch to show how we processed the data. The intensity values were normalized against the average mean intensity before bleaching. (C, D, E) Quantification of the  $t_{1/2}$ , mobile fraction, and immobile fraction. A total of 30 condensates from 30 separate cells were photobleached, and their recovery profiles were fitted to the exponential recovery equation (see Methods for details). "All" indicates the summation of data without regard to droplet size. In addition, we analyzed the droplets as separated into small, medium, and large groups (see S6 Fig for more information about how this separation was performed). (C) provides a numerical summary of the  $t_{1/2}$ , mobile fraction, and immobile fraction. Panel (D) provides a box plot of the

 $t_{1/2}$  of each size group, while panel (E) provides a bar graph of the fractions of mobile and immobile protein. n=14 (Small), 11 (Medium), and 5 (Large), for a total of 30 droplets. The error bars show the standard deviation; other aspects of the box plot are as generated by the default Excel Box and Whisker plot function. N.S. = Not Significant (there were no significant differences between any of these groups).

To further understand the kinetics of CLIP-170 patches, we categorized our FRAP data into three groups by patch diameter to determine whether the fluorescence recovery time and/or degree varied with size: small (0 – 2.4  $\mu$ m), medium (2.4 – 4.4  $\mu$ m), and large ( $\geq$  4.4  $\mu$ m). The grouping strategy is based on the size distribution after measuring the diameters of ~300 condensates (S6 Fig).

We observed that while the recovery of the medium patches was more variable than that of large and small patches, there was no significant difference between the groups in either the recovery rate or recovery extent (Figs 6C-E). These observations are notable for three reasons. First, since bleaching generally covered the full area of the small patches, the observation that small patches recover quickly confirms that the patches are not membrane bound because the interior of a membrane-bound compartment would not be expected to exchange material with the cytoplasm (exterior) on this time scale. Second, the observation that all three patch sizes recover with a similar rate indicates that the surface area: volume ratio is not rate limiting for material exchange with the cytoplasm. This in turn suggests that the patches are relatively porous. Third, the observation that the size of the condensates does not obviously correlate with the observed exchange dynamics is consistent with the idea that the CLIP-170 patches may reflect processes occurring in the small, endogenous +TIP network comets ( $\sim$ 0.5  $\mu$ m).

Taken together, our results thus far demonstrate that the CLIP-170 patches share key properties with known biomolecular condensates: they are membraneless, they undergo elastic deformations, fission, and fusion, they selectively include some molecules (e.g., +TIPs) while excluding others (e.g., stress granule proteins), and proteins exchange rapidly between patches and the cytoplasm. These observations lead us to conclude that the CLIP-170-induced patches are biomolecular condensates.

610 611 Sequence information is consistent with the idea that CLIP-170 is a component of 612 biomolecular condensates 613 614 If CLIP-170 is inducing biomolecular condensates, one would expect CLIP-170 to have 615 sequence attributes consistent with this activity. As mentioned above, proteins found in 616 condensates (i.e., proteins that have the potential to undergo phase-phase separation) 617 typically are multivalent (i.e., have multiple binding sites for other biomolecules) and 618 contain intrinsically disordered regions (IDRs). Indeed, it is already well-established in 619 the literature that CLIP-170 has multivalent interactions with multiple other proteins: a 620 dimer of CLIP-170 has as many as ten binding sites for tubulin (15), multiple binding sites 621 for EB1 (16), and an array of binding sites for other proteins including p150 (reviewed by 622 (3)). However, while it seems widely known that CLIP-170 contains IDRs, we were not 623 able to find a formal analysis of this question in the literature. 624 625 Therefore, we evaluated the sequence of human CLIP-170 for the presence of 626 disordered regions by using the established predictors "ESpritz version 1.3" (50), 627 "MobiDB-lite" (51), and "IUPred" (52). In parallel, we used the "COILS" server to delineate the coiled-coil region (Fig 7) because we wanted to focus on IDR predictions 628 629 outside of likely coiled-coil; this was important because in preliminary work, some 630 predictors (e.g., PONDR) frequently identified coiled-coil regions as likely IDRs (see also 631 (63)). These analyses show that the three serine-rich regions in the N-terminal domain 632 and regions adjacent to the zinc-knuckles in the C-terminal domain are predicted to be 633 disordered in human CLIP-170 (Fig 7). 634 635 Fig 7. Analysis of coiled-coil domains and IDRs for human CLIP-170 (AAA35693.1). (Top) CLIP-170 domain 636 structure summary. The N-terminal domain includes the 2 CAP-Gly domains and 3 serine-rich regions. The 637 coiled-coil domain is labeled in orange, and its boundaries are indicated with two red lines. The C-terminal 638 domain contains two zinc-knuckle motifs (yellow). (Middle) Analysis of coiled-coil propensity as predicted 639 by COILS. The colored lines represent the probability that a region assumes a coiled-coil conformation, as 640 assessed for different windows (7AA, blue; 14 AA, orange; 21 AA yellow), with 1 on the Y-axis indicating 641 100% likelihood. (Bottom) IDR predictions (Y-axis) as function of amino acid position (X-axis), with 1

indicating 100% likelihood. The purple line represents the probability of IDRs as predicted by Espritz, with red arrows indicating the 10 regions predicted to be disordered. The grey areas indicate the IDRs as predicted by MobiDB-lite. The green line represents the probability of IDRs as predicted by IUPred2A, and the light green indicates the probability of 0.5.

The observations that CLIP-170 is multivalent (3, 15, 16) and contains IDRs (Fig 7) are consistent with the idea that CLIP-170 can participate in biomolecular condensates. If these attributes are functionally significant, they should be conserved in diverse organisms. Indeed, examination of CLIP-170 relatives shows that the domain structure of CLIP-170 is conserved across diverse organisms (Fig 8 and S7 Fig), as previously noted in many publications; conservation of the domain structure implies conservation of multivalency. Moreover, our analysis demonstrates that the presence of IDRs adjacent to the CAP-Gly motifs and zinc knuckles is also well-conserved, extending even to the yeasts *S. cerevisiae* and *S. pombe* (Fig 8 and S7 Fig).

Fig 8. Analysis of coiled-coil and IDRs in CLIP-170 relatives from a range of different species. For each organism listed, one representative CLIP-170 sequence was selected for analysis, the results of which are shown in three images. The set of upper images provides the domain structure for each sequence, with colors as indicated: blue: CAP-Gly domains; orange: coiled-coil regions; pink: FEED domain; yellow: zinc-knuckle motifs. The sets of middle and lower images respectively provide the probabilities that a region is coiled-coil (as predicted by COILS) or IDR (as predicted by Espritz). For both analyses, 1 indicates 100% likelihood and \* indicates the end of the sequence.

Two additional points are relevant to interpreting these data. First, though IDRs are not universally detected in the same places in all the organisms shown, assignment of IDRs is still an imperfect process; it remains possible that some of the proteins that appear to lack IDRs in particular regions (e.g., serine-rich 3 of Drosophila, the post-CAP-Gly serine-rich region of *S. pombe*) actually have them. Second, IDRs are sometimes identified in the coiled-coil regions, consistent with the established propensity of IDR prediction programs to find predicted IDRs in coiled-coil (63). The observation that these predicted IDRs are less conserved in their positions than are the IDRs near the CAP-Gly domains and zinc knuckles suggests that these may be spurious assignments.

In conclusion, the sequence characteristics of CLIP-170 and its relatives are consistent with the idea that CLIP-170 participates in biomolecular condensates and that this activity is conserved across a wide range of organisms.

#### IDRs in other +TIP proteins are both common and conserved

Thus far, our analyses have focused on CLIP-170 and the condensates induced by CLIP-170 overexpression. As discussed in the Introduction, we are interested in the possibility that these large induced condensates reflect a much smaller +TIP network structure that exists under normal conditions, on the MT +TIP and/or in other cellular locations. Our sequence analyses (Fig 8 and S7 Fig) suggest that the ability of CLIP-170 to participate in condensates is likely to be conserved from humans to yeast, consistent with the idea that condensate formation is functionally significant. However, CLIP-170 can be deleted from some organisms (e.g., *S. cerevisiae*) with relatively minor effects (S1 Table), and other organisms (e.g., *Dictyostelium* amoebas, plants) lack CLIP-170 entirely, arguing against a central role for CLIP-170 in function of the +TIP network.

These observations indicate that if the normal activities of the +TIP network involve a functionally significant biomolecular condensate, other +TIPs should be able to drive condensate formation. Addressing this question in depth is beyond the scope of this paper. However, as a first step, we examined the sequences of other +TIPs to see if they have characteristics consistent with condensate formation, i.e., multivalency and the presence of IDRs. As noted above, it is already well-established that many human +TIPs are multivalent (3). Therefore, we examined the sequences of other human +TIPs to see if they contain IDRs. As part of this analysis, we included other proteins that colocalized with CLIP-170 from our immunofluorescence study (Fig 9).

**Fig 9. Analyses of IDRs in members of the human +TIP network.** The Y-axis provides the probability of IDRs as a function of amino acid position (X-axis); 1 indicates 100% likelihood. The purple line provides the data for Espritz; shaded areas are the disordered regions predicted by MobiDB-lite. See Materials and Methods for the accession numbers.

Our analyses show that the human versions of proteins that colocalized with CLIP-170 patches (EB1, LIS1, CLASP1, CLASP2, mDia2, and p150) contain predicted IDRs, as do other common +TIPs (APC and MAP215). As part of this work, we also examined sequences for the presence of alpha helical coiled-coil (using the COILS server) and the other conserved domains (using hmmscan to search the PFAM database). Comparison of these results with the IDR predictions shows that the predicted disordered regions are mostly outside of alpha-helical coiled-coil and recognized folded domains (e.g. the CH domain in EB1) (S8 Fig), consistent with the idea that the IDR predictions are accurate. Although prediction of IDRs from sequence information is still maturing, and though presence of IDRs in a protein does not necessarily indicate that the protein participates in condensate formation, our results show that IDRs are very common in proteins involved in the +TIP network.

If the IDRs are functionally significant, their presence and perhaps also their positions relative to other conserved domains should be conserved across divergent organisms. To test these predictions, we chose the three most ubiquitous and conserved +TIPs (EB1, MAP215, and CLASPs) and examined their sequences for the presence of IDRs and recognized domains in organisms ranging from humans to plants. The results (S9-S11 Figs) show that both the presence and position of disordered regions is well-conserved in all three proteins throughout all of the species examined.

More specifically, in EB1 (S9 Fig), both MobiDB-lite and Espritz predict a disordered region for all species examined upstream of the coiled-coiled region, between the CH and EBH domains. The Espritz predictor also predicts a disordered region after the EBH domain for all species (S9 Fig). In MAP215, both predictors find disordered regions outside of the TOG regions. The pattern of disordered regions is surprisingly similar for MAP215 in all species, except in yeast, where the length of the MAP215 homologs is dramatically reduced (S10 Fig). In CLASP, the presence and position of disordered regions are highly conserved from human to fly. The similarity of the domain structures is less obvious in yeast, *Dictyostelium*, and plants, but it is notable that the CLASP homologs in all of these organisms still contain IDRs (S11 Fig).

738 In conclusion, analysis of the protein sequences demonstrates that CLIP-170 and other 739 members of the +TIP network have IDRs, consistent with participation of these proteins 740 in biomolecular condensates. Moreover, the presence and position of these IDRs is well-741 conserved across animals and (where relevant) to organisms as divergent as plants, 742 indicating that these IDRs are functionally significant. Moreover, the observation that 743 the general domain structure of key +TIPs is conserved in organisms as diverse as plants 744 (Fig 8 and S9-11 Figs) indicates that multivalency is also likely to be a conserved feature. 745 These observations are consistent with the hypothesis that the +TIP network can 746 assemble into a functionally significant biomolecular condensate. **Discussion** 747 748 The "patches" induced by CLIP-170 are biomolecular condensates 749 Our results demonstrate that the so-called "patches" induced by CLIP-170 750 overexpression (8, 19) have the key hallmarks of biomolecular condensates (i.e., 751 structures formed by liquid-liquid phase separation): elastic deformability (Fig 3 and 752 Movies 3-4), the ability to undergo fission and fusion (Fig 3 and Movies 3-4), selective 753 inclusion of some proteins and exclusions of others (Figs 4-5, S3-4 Figs, and Table 1), and 754 rapid protein exchange with the cytoplasm (Fig 6). These observations lead us to 755 conclude that the patches are biomolecular condensates. Significantly, the lack of 756 overlap with established condensate markers (Fig 4 and S3 Fig) also suggests that the 757 patches may represent a previously unrecognized type of condensate. 758 759 While these observations indicate that the CLIP-170-induced structures are 760 biomolecular condensates, they do not address the question of functional significance. 761 One possibility is that the overexpression-induced +TIP condensates are simply 762 overexpression artifacts (albeit ones based on specific interactions) and so have no 763 functional significance. Alternatively, the +TIP condensates observed in overexpression 764 experiments could reflect +TIP superstructures that are formed by the endogenous +TIP 765 network. In this regard, it is significant that the ability of overexpressed CLIP-170 to 766 drive condensate formation depends on the protein having both an intact second zinc 767 knuckle domain (See Fig 4 in (19)) as well as a free C-terminus (S1 Fig). These

observations indicate that condensate formation is specific and is not a generic outcome

of protein overexpression, but they do not directly address the question of physiological significance.

Resolving this question would be challenging, in part because the comet at the end of MTs in unperturbed cells is both small (near the diffraction limit in size) and very dynamic. Moreover, a functionally significant +TIP condensate could form in environments other than the plus-end comet (e.g., at the cell cortex). For these reasons, directly testing the hypothesis that +TIP condensate formation is functionally relevant is beyond the scope of this work. However, as a first step in this direction, we examined CLIP-170 and other +TIPs for the presence of sequence characteristics (specifically multivalency and the presence of IDRs) consistent with participation in condensates. We then investigated how conserved these characteristics are across evolution. Finding out whether condensate-associated sequence characteristics are common in human +TIP network proteins was intended to answer the question of whether condensate participation is a general feature +TIP network proteins or more specific to CLIP-170. The conservation analysis was performed as a test of functional significance, since a feature that impacts function of a basic cell biological process would be expected to be maintained across evolution.

As known from previous work (3, 15, 16), multivalency is indeed common in +TIPs (see also Fig 8 and S9-S11 Figs). Importantly, conservation of the basic domain structure of these proteins across wide spans of evolution (Fig 8 and S9-S11 Figs) indicates that multivalency is also a conserved feature of these proteins. In addition, we observed that IDRs are common in +TIPs (Fig 9 and S8 Fig). Significantly, for key +TIPs that can be recognized in divergent organisms, the existence and position of these predicted IDRs is also well-conserved across wide spans of evolution (e.g. humans through plants, Fig 8 and S9-S11 Figs), suggesting that these domains have activities that are functionally significant.

In considering these observations, it is important to stress that it is the existence and position of the predicted IDRs relative to conserved domains that are conserved, not the linear sequence of these predicted IDR-domains themselves. Indeed, at a primary

sequence level, the regions identified as IDRs typically align poorly, once organisms outside of animals are compared (e.g., S7 Fig). Although one might be tempted to conclude that the poor alignability of these regions suggests lack of functional significance, it is instead consistent with the idea that these regions of the +TIPs are intrinsically disordered (64). In conclusion, our sequence analysis indicates that multiple members of the +TIP network have sequence features consistent with condensate formation and that these features are largely conserved across evolution, providing evidence that +TIP condensate formation is functionally significant.

One important question raised by the observations above is whether overexpression of other +TIPs causes condensate formation. We are not aware of other reports in the literature where overexpression of +TIPs has led to formation of structures characterized to be or described as condensates or liquid droplets. Significantly, in our hands, overexpression of EB1 (tagged at either end or untagged) does not lead to patch formation (19). However, some reports of condensate formation by other +TIPs have appeared in unpublished meeting abstracts. Most strikingly, overexpression of full-length APC has been described as causing formation of "granules" or "aggregates" that dynamically track growing MT plus ends but differ in appearance from typical +TIP comets; these structures exhibit behaviors that to us are strongly suggestive of liquid condensates (see e.g., Fig 6 and Fig 6a-6c videos in (65)). Thus, there is reason to expect that other +TIPs can promote condensate formation as well.

So, starting from the recognition that we do not yet know whether +TIP condensate formation is physiologically significant, how *might* it be physiologically significant? As discussed more below, we propose that condensate formation may be fundamental to the core function of the +TIP network in regulating MT dynamics. As a foundation for discussing this hypothesis, we first review established functions for condensates and briefly review what is known about the mechanism of MT dynamic instability and its regulation by MT binding proteins.

#### Functions of established biomolecular condensates

Before considering how a +TIP condensate might function, it is useful to first examine functions of other condensates. As discussed in the Introduction, the function of condensates is typically less clear than their existence. However, two commonly proposed functions are concentrating biomolecules to promote reactions (e.g., (37)) and segregating biomolecules into storage depots to prevent unwanted reactions (e.g., (25)). Both functions involve using condensates to alter the concentrations of reactants and thus the rates or timing of reactions. A very different set of proposed functions involves the ability of condensates to resist mechanical force (38) or even generate it (66). Though sometimes left out of discussions of condensate function, is not surprising that assembly of condensates (which could be considered a type of 3D polymerization) would be able to generate mechanical force, given the well-demonstrated ability of actin and tubulin polymerization to generate force (67, 68). Finally, another set of proposed functions for condensates, one which overlaps with the ideas above, is that they play a role in signal transduction (69). Indeed, one could imagine that a phase separated droplet, a local region of high concentration that is in communication with the rest of the cell, could be an ideal structure for integrating information from multiple pathways, helping the cell to produce a coherent response to conflicting signals (70).

While it is now well-known that condensates are important for processes such as stress response and RNA processing, recent work also indicates that condensate formation plays a fundamental role in cytoskeletal processes. For example, phase separation appears to play an important role in regulation of actin nucleation (71-73). In the MT cytoskeleton, there is evidence that condensates are important to both the normal function of the MT binding protein Tau and its role in neurodegenerative disease (34-36). Moreover, one of the most striking existing examples of functionally significant cytoplasmic condensates is the centrosome, where condensate formation helps to both concentrate and localize the MT nucleating machinery and resist the forces generated during cell division (38). Here we consider possible roles for a condensate composed of +TIP proteins.

864 Mechanism of MT dynamic instability and its regulation by MT binding proteins 865 To consider possible functions for +TIP condensates and how they might regulate MT 866 dynamic instability (DI), it is first necessary to consider the mechanism of DI. MT growth 867 and shrinkage result from the incorporation and detachment of tubulin dimers at 868 protofilament ends exposed on MT tips. The details of the mechanism of DI are still 869 being elucidated, but models center around the observation that tubulin subunits bind 870 GTP but hydrolyze it soon after hydrolysis; this and other work have led to the idea that 871 MTs can grow as long as they maintain a cap of GTP tubulin but switch to 872 depolymerization (i.e., undergo "catastrophe") if they lose this cap through stochastic 873 GTP hydrolysis or other mechanisms (reviewed by (2)). 874 875 Additional detail in the process is provided by recent electron microscopy indicating that 876 growing MTs have extended protofilaments that are laterally unbound near the tip (74). 877 This observation suggests that protofilaments need to "zip up" to be fully incorporated 878 into the MT, and thus that the tip might be both fragile and very dynamic. Though 879 surprising to some, the existence of laterally unbound protofilaments was predicted by 880 a dimer scale computational model (75), and it is consistent with biophysical 881 experiments that indicate that subunits exchange rapidly at the tip (76). 882 883 An important and puzzling observation is that MTs in vivo grow ~5x faster than those in 884 vitro, even when tubulin concentrations have been matched (77). Remarkably, mixtures 885 of +TIPs (specifically EB1 and MAP215) can reconstitute in vivo rates of polymerization in 886 vitro (7). Two explanations have been offered for how the proteins are able to enhance 887 the growth rates so much. One possibility is that MAP215 and its relatives enhance the 888 addition of new tubulin subunits to the tip, e.g., by binding and "delivering" tubulin 889 subunits (78). The other possibility is that the proteins increase the rate of growth by 890 reducing the fraction of tubulin subunits that detach after binding (4, 79). 891 892 Though less intuitive, this second mechanism is attractive as an explanation for the 893 dramatic effect of +TIPs, especially when combined with evidence that MT tips have 894 laterally unbound protofilaments (74). Briefly, the observation mentioned above that 895 incoming tubulin subunits "exchange rapidly at the tip" means that most incoming

subunits detach instead of becoming incorporated into the lattice (76). A protein that could prevent detachment could dramatically increase the rate of polymerization (79). Laterally unbound protofilaments as discussed above might be expected to break off in chunks. Thus, one straightforward way for +TIPs to enhance the net growth rate so dramatically would be to prevent detachment by zipping up the bonds between protofilaments (4).

# Hypothesis: the +TIP network forms a condensate that coats the MT tip, creating a superstructure that acts as a polymerization chaperone

As mentioned above, our lab has previously proposed that the web of +TIP interactions may have a physical purpose, creating a superstructure that promotes MT polymerization by stabilizing the weak lateral interactions between protofilaments, thus increasing the fraction of incoming subunits that are incorporated into the lattice (4). Here we extend this hypothesis by proposing that the +TIP network superstructure referred to in this original hypothesis is a biomolecular condensate. More specifically, we suggest that the endogenous +TIP network can form a stocking-like structure that acts as a polymerization chaperone by encircling the MT tip in a supportive web, increasing the rate of lateral bond formation between protofilaments, which in turn decreases the rate of subunit detachment and thus increases the overall rate of MT growth (Fig 10).

Fig 10. Proposed polymerization chaperone model. (A) In absence of the +TIP network, tubulin subunits arrive and leave quickly because most newly attached subunits are initially in the laterally unbonded regions of the tip protofilaments. The result is that MTs grow relatively slowly because most subunits detach before being incorporated into the laterally bound region of the MT. (B) In the presence of the proposed +TIP network liquid droplet, the web of interactions between the +TIPs creates a dynamic stocking-like structure that tracks the tip by diffusing on the potential energy gradient created by the preferential affinity of some tip components (most notably EB1) for tip-specific tubulin conformations. As the droplet moves, it exerts a force on the tip that promotes the zipping up of lateral bonds between protofilaments. This effect in turn increases the likelihood that newly arrived subunits are incorporated into the lattice and enables the MT to grow faster, as seen *in vivo* or with mixtures of +TIPs *in vitro* (4). This figure was created with BioRender (5).

As indicated in Fig 10, such a structure could potentially track the growing end by diffusing on the "wave" formed by the GTP (or GDP-Pi) cap, e.g., as has been proposed for proteins such as MAP215 (80). Alternatively, one could also imagine +TIP droplet superstructure having utility if placed in a specific static position on a MT, such as has been suggested for Tau condensates (36).

Whether +TIP comets necessarily correspond to condensates is not specified in our hypothesis. Indeed, one piece of evidence against the idea that all +TIPs comets involve condensates is that researchers performing FRAP of MT comets using diffraction-limited spots measured a  $t_{1/2}$  of ~0.2 sec (81). This number is ~40 times faster than the  $t_{1/2}$  we observed for the CLIP-170 induced condensates (~8.5 sec). Regardless, even if the +TIP network on the average MT tip is not a condensate, one might expect that condensate formation could be triggered locally from +TIP-localized proteins in response to appropriate signals. One locale where the possibility of +TIP condensate formation seems particularly intriguing is at the kinetochore-MT attachment site, given that a number of +TIP proteins localize to kinetochores and that condensate formation at the kinetochore has already been suggested (82). Indeed, the evidence cited above that condensates can generate mechanical force (66) is particularly striking when considered in the context of evidence that pulling forces on kinetochore components can promote MT growth (83, 84).

In considering the potential function and regulation of +TIP condensate formation, it is notable that the CLIP-170-induced patches are frequently found away from MT plus ends (Figs 2 and 5, and S4 Fig), and that they persist in the presence of the MT-depolymerizing drug nocodazole (Fig 5). Moreover, the observation that patches form in cells exposed to nocodazole after only eight hours of transfection (Fig 5) raises the possibility that patches may be able to form in the absence of MTs. These observations could be used to argue that the patches are independent of MTs, initially providing evidence against the polymerization chaperone model for condensate function.

However, it is important to remember that condensates generally have a critical concentration for assembly, meaning that when constituents are present at concentrations above this value, condensates form spontaneously (85). Significantly, the value of this critical concentration could potentially be influenced by factors including the presence of a platform for assembly and/or post-translational modifications that influence the interactions between subunits of the condensate (85). Thus, we explain the observation that patches exist apart from MT tips and persist (and perhaps even form) in nocodazole by speculating that under normal physiological conditions, the MT tip or some other structure (e.g, the kinetochore) acts as a platform to locally nucleate +TIP condensate formation. However, under CLIP-170 overexpression conditions, the critical concentration for spontaneous assembly is surpassed, allowing condensates to exist independently of MTs. How potential platforms (including MT tips) and/or regulatory mechanisms influence +TIP condensate formation is an interesting topic for future work.

## **Conclusion**

In summary, we have shown that "patches" induced by CLIP-170 overexpression are biomolecular condensates. The overexpression approach, although artificial, may still give us insight into the mechanism of the physiological +TIP network. Initial support for the idea that condensate formation is functionally significant is provided by our bioinformatics studies, which have shown that CLIP-170 and other members of the +TIP network have conserved IDRs. This evidence leads us to propose that the endogenous +TIP network can under appropriate conditions form a dynamic stocking-like condensate that zips up the lateral bonds between protofilaments to promote MT polymerization.

# Acknowledgements

- We are grateful to the Optical Microscopy Core/NDIIF, University of Notre Dame, for the
- use of their instruments and services in support of this work. This research was funded
- 988 by a fellowship from the American Heart Association (#17PRE33670896) to YOW and a
- 989 grant from the National Science Foundation (MCB #1817966) to HVG.

# Reference

985

- 991 1. Matamoros AJ, Baas PW. Microtubules in health and degenerative disease of the 992 nervous system. Brain Res Bull. 2016;126(Pt 3):217-25.
- 993 2. Goodson HV, Jonasson EM. Microtubules and Microtubule-Associated Proteins. Cold
- 994 Spring Harb Perspect Biol. 2018;10(6).
- 995 3. Akhmanova A, Steinmetz MO. Control of microtubule organization and dynamics:
- two ends in the limelight. Nat Rev Mol Cell Biol. 2015;16(12):711-26.
- 997 4. Gupta KK, Alberico EO, Nathke IS, Goodson HV. Promoting microtubule assembly: A
- hypothesis for the functional significance of the +TIP network. Bioessays.
- 999 2014;36(9):818-26.
- 1000 5. BioRender. 2020. Available from: https://biorender.com/.
- 1001 6. Li W, Moriwaki T, Tani T, Watanabe T, Kaibuchi K, Goshima G. Reconstitution of
- dynamic microtubules with *Drosophila* XMAP215, EB1, and Sentin. J Cell Biol.
- 1003 2012;199(5):849-62.
- 1004 7. Zanic M, Widlund PO, Hyman AA, Howard J. Synergy between XMAP215 and EB1
- increases microtubule growth rates to physiological levels. Nat Cell Biol.
- 1006 2013;15(6):688-93.
- 1007 8. Pierre P, Scheel J, Rickard JE, Kreis TE. CLIP-170 links endocytic vesicles to
- 1008 microtubules. Cell. 1992;70(6):887-900.
- 1009 9. Pierre P, Pepperkok R, Kreis TE. Molecular characterization of two functional
- domains of CLIP-170 in vivo. J Cell Sci. 1994;107 ( Pt 7):1909-20.
- 1011 10. Lomakin AJ, Kraikivski P, Semenova I, Ikeda K, Zaliapin I, Tirnauer JS, et al.
- Stimulation of the CLIP-170--dependent capture of membrane organelles by
- microtubules through fine tuning of microtubule assembly dynamics. Mol Biol Cell.
- 1014 2011;22(21):4029-37.

- 1015 11. Komarova YA, Akhmanova AS, Kojima S, Galjart N, Borisy GG. Cytoplasmic linker proteins promote microtubule rescue *in vivo*. J Cell Biol. 2002;159(4):589-99.
- 1017 12. Henty-Ridilla JL, Rankova A, Eskin JA, Kenny K, Goode BL. Accelerated actin filament polymerization from microtubule plus ends. Science. 2016;352(6288):1004-9.
- 1019 13. Lewkowicz E, Herit F, Le Clainche C, Bourdoncle P, Perez F, Niedergang F. The
- 1020 microtubule-binding protein CLIP-170 coordinates mDia1 and actin reorganization
- during CR3-mediated phagocytosis. J Cell Biol. 2008;183(7):1287-98.
- 1022 14. Noritake J, Watanabe T, Sato K, Wang S, Kaibuchi K. IQGAP1: a key regulator of adhesion and migration. J Cell Sci. 2005;118(Pt 10):2085-92.
- 1024 15. Gupta KK, Paulson BA, Folker ES, Charlebois B, Hunt AJ, Goodson HV. Minimal plus-
- end tracking unit of the cytoplasmic linker protein CLIP-170. J Biol Chem.
- 1026 2009;284(11):6735-42.
- 16. Chen Y, Wang P, Slep KC. Mapping multivalency in the CLIP-170-EB1 microtubule plus-end complex. J Biol Chem. 2019;294(3):918-31.
- 1029 17. Scheel J, Pierre P, Rickard JE, Diamantopoulos GS, Valetti C, van der Goot FG, et al.
- Purification and analysis of authentic CLIP-170 and recombinant fragments. J Biol
- 1031 Chem. 1999;274(36):25883-91.
- 1032 18. Mishima M, Maesaki R, Kasa M, Watanabe T, Fukata M, Kaibuchi K, et al. Structural
- basis for tubulin recognition by cytoplasmic linker protein 170 and its
- autoinhibition. Proc Natl Acad Sci U S A. 2007;104(25):10346-51.
- 1035 19. Goodson HV, Skube SB, Stalder R, Valetti C, Kreis TE, Morrison EE, et al. CLIP-170
- interacts with dynactin complex and the APC-binding protein EB1 by different
- mechanisms. Cell Motil Cytoskeleton. 2003;55(3):156-73.
- 1038 20. Weisbrich A, Honnappa S, Jaussi R, Okhrimenko O, Frey D, Jelesarov I, et al.
- 1039 Structure-function relationship of CAP-Gly domains. Nat Struct Mol Biol.
- 1040 2007;14(10):959-67.
- 1041 21. Banani SF, Lee HO, Hyman AA, Rosen MK. Biomolecular condensates: organizers of
- cellular biochemistry. Nat Rev Mol Cell Biol. 2017;18(5):285-98.
- 1043 22. Alberti S, Gladfelter A, Mittag T. Considerations and Challenges in Studying Liquid-
- 1044 Liquid Phase Separation and Biomolecular Condensates. Cell. 2019;176(3):419-34.
- 1045 23. Bracha D, Walls MT, Brangwynne CP. Probing and engineering liquid-phase
- organelles. Nat Biotechnol. 2019;37(12):1435-45.

- 1047 24. Ditlev JA, Case LB, Rosen MK. Who's In and Who's Out-Compositional Control of
- 1048 Biomolecular Condensates. J Mol Biol. 2018;430(23):4666-84.
- 1049 25. Brangwynne CP, Eckmann CR, Courson DS, Rybarska A, Hoege C, Gharakhani J, et al.
- Germline P granules are liquid droplets that localize by controlled
- 1051 dissolution/condensation. Science. 2009;324(5935):1729-32.
- 1052 26. Kulkarni M, Ozgur S, Stoecklin G. On track with P-bodies. Biochem Soc Trans.
- 1053 2010;38(Pt 1):242-51.
- 1054 27. Sear RP. Dishevelled: a protein that functions in living cells by phase separating. Soft
- 1055 Matter. 2007;3(6):680-4.
- 1056 28. Scheer U, Hinssen H, Franke WW, Jockusch BM. Microinjection of actin-binding
- proteins and actin antibodies demonstrates involvement of nuclear actin in
- transcription of lampbrush chromosomes. Cell. 1984;39(1):111-22.
- 1059 29. Gammons M, Bienz M. Multiprotein complexes governing Wnt signal transduction.
- 1060 Curr Opin Cell Biol. 2018;51:42-9.
- 1061 30. Woodruff JB, Ferreira Gomes B, Widlund PO, Mahamid J, Honigmann A, Hyman AA.
- The Centrosome Is a Selective Condensate that Nucleates Microtubules by
- 1063 Concentrating Tubulin. Cell. 2017;169(6):1066-77 e10.
- 1064 31. Rale MJ, Kadzik RS, Petry S. Phase Transitioning the Centrosome into a Microtubule
- 1065 Nucleator. Biochemistry. 2018;57(1):30-7.
- 1066 32. Cioce M, Lamond AI. Cajal bodies: a long history of discovery. Annu Rev Cell Dev
- 1067 Biol. 2005;21:105-31.
- 1068 33. Lallemand-Breitenbach V, de The H. PML nuclear bodies. Cold Spring Harb Perspect
- 1069 Biol. 2010;2(5):a000661.
- 1070 34. Wegmann S, Eftekharzadeh B, Tepper K, Zoltowska KM, Bennett RE, Dujardin S, et
- al. Tau protein liquid-liquid phase separation can initiate tau aggregation. EMBO J.
- 1072 2018;37(7).
- 1073 35. Ambadipudi S, Biernat J, Riedel D, Mandelkow E, Zweckstetter M. Liquid-liquid
- phase separation of the microtubule-binding repeats of the Alzheimer-related
- 1075 protein Tau. Nat Commun. 2017;8(1):275.
- 1076 36. Tan R, Lam AJ, Tan T, Han J, Nowakowski DW, Vershinin M, et al. Microtubules gate
- tau condensation to spatially regulate microtubule functions. Nat Cell Biol.
- 1078 2019;21(9):1078-85.

- 1079 37. Snead WT, Gladfelter AS. The Control Centers of Biomolecular Phase Separation:
- How Membrane Surfaces, PTMs, and Active Processes Regulate Condensation. Mol
- 1081 Cell. 2019;76(2):295-305.
- 1082 38. Mittasch M, Tran VM, Rios MU, Fritsch AW, Enos SJ, Ferreira Gomes B, et al.
- 1083 Regulated changes in material properties underlie centrosome disassembly during
- 1084 mitotic exit. J Cell Biol. 2020;219(4).
- 1085 39. Choi JM, Holehouse AS, Pappu RV. Physical Principles Underlying the Complex
- Biology of Intracellular Phase Transitions. Annu Rev Biophys. 2020;49:107-33.
- 1087 40. Diamantopoulos GS, Perez F, Goodson HV, Batelier G, Melki R, Kreis TE, et al.
- Dynamic localization of CLIP-170 to microtubule plus ends is coupled to microtubule
- 1089 assembly. J Cell Biol. 1999;144(1):99-112.
- 1090 41. Perez F, Diamantopoulos GS, Stalder R, Kreis TE. CLIP-170 highlights growing
- 1091 microtubule ends *in vivo*. Cell. 1999;96(4):517-27.
- 1092 42. Rickard JE, Kreis TE. Binding of pp170 to microtubules is regulated by
- 1093 phosphorylation. J Biol Chem. 1991;266(26):17597-605.
- 1094 43. Simonsen A, Lippe R, Christoforidis S, Gaullier JM, Brech A, Callaghan J, et al. EEA1
- links PI(3)K function to Rab5 regulation of endosome fusion. Nature.
- 1096 1998;394(6692):494-8.
- 1097 44. Kawano J, Ide S, Oinuma T, Suganuma T. A protein-specific monoclonal antibody to
- rat liver beta 1-->4 galactosyltransferase and its application to
- immunohistochemistry. J Histochem Cytochem. 1994;42(3):363-9.
- 1100 45. Schindelin J, Arganda-Carreras I, Frise E, Kaynig V, Longair M, Pietzsch T, et al. Fiji: an
- open-source platform for biological-image analysis. Nat Methods. 2012;9(7):676-82.
- 46. Webster AW, M. An easy protocol for FRAP 2014. Available from:
- http://www.its.caltech.edu/~bif/Public/An%20Easy%20Protocol%20for%20FRAP.do
- 1104 cx.
- 1105 47. Bulinski JC, Odde DJ, Howell BJ, Salmon TD, Waterman-Storer CM. Rapid dynamics
- of the microtubule binding of ensconsin *in vivo*. J Cell Sci. 2001;114(Pt 21):3885-97.
- 48. Sprague BL, Pego RL, Stavreva DA, McNally JG. Analysis of binding reactions by
- fluorescence recovery after photobleaching. Biophys J. 2004;86(6):3473-95.
- 49. Wachsmuth M. Molecular diffusion and binding analyzed with FRAP. Protoplasma.
- 1110 2014;251(2):373-82.

- 1111 50. Walsh I, Martin AJ, Di Domenico T, Tosatto SC. ESpritz: accurate and fast prediction
- of protein disorder. Bioinformatics. 2012;28(4):503-9.
- 1113 51. Necci M, Piovesan D, Dosztanyi Z, Tosatto SCE. MobiDB-lite: fast and highly specific
- consensus prediction of intrinsic disorder in proteins. Bioinformatics.
- 1115 2017;33(9):1402-4.
- 1116 52. Meszaros B, Erdos G, Dosztanyi Z. IUPred2A: context-dependent prediction of
- protein disorder as a function of redox state and protein binding. Nucleic Acids Res.
- 1118 2018;46(W1):W329-W37.
- 1119 53. Erdos G, Dosztanyi Z. Analyzing Protein Disorder with IUPred2A. Curr Protoc
- 1120 Bioinformatics. 2020;70(1):e99.
- 1121 54. Potenza E, Di Domenico T, Walsh I, Tosatto SC. MobiDB 2.0: an improved database
- of intrinsically disordered and mobile proteins. Nucleic Acids Res. 2015;43(Database
- 1123 issue):D315-20.
- 55. Sievers F, Wilm A, Dineen D, Gibson TJ, Karplus K, Li W, et al. Fast, scalable
- generation of high-quality protein multiple sequence alignments using Clustal
- 1126 Omega. Mol Syst Biol. 2011;7:539.
- 1127 56. Mirarab S, Nguyen N, Guo S, Wang LS, Kim J, Warnow T. PASTA: Ultra-Large Multiple
- Sequence Alignment for Nucleotide and Amino-Acid Sequences. J Comput Biol.
- 1129 2015;22(5):377-86.
- 1130 57. Potter SC, Luciani A, Eddy SR, Park Y, Lopez R, Finn RD. HMMER web server: 2018
- 1131 update. Nucleic Acids Res. 2018;46(W1):W200-W4.
- 1132 58. Lupas A, Van Dyke M, Stock J. Predicting coiled coils from protein sequences.
- 1133 Science. 1991;252(5009):1162-4.
- 1134 59. Folker ES, Baker BM, Goodson HV. Interactions between CLIP-170, tubulin, and
- 1135 microtubules: implications for the mechanism of Clip-170 plus-end tracking
- 1136 behavior. Mol Biol Cell. 2005;16(11):5373-84.
- 1137 60. Bartolini F, Moseley JB, Schmoranzer J, Cassimeris L, Goode BL, Gundersen GG. The
- formin mDia2 stabilizes microtubules independently of its actin nucleation activity. J
- 1139 Cell Biol. 2008;181(3):523-36.
- 1140 61. Namkoong S, Ho A, Woo YM, Kwak H, Lee JH. Systematic Characterization of Stress-
- 1141 Induced RNA Granulation. Mol Cell. 2018;70(1):175-87 e8.
- 1142 62. McSwiggen DT, Mir M, Darzacq X, Tjian R. Evaluating phase separation in live cells:

- diagnosis, caveats, and functional consequences. Genes Dev. 2019;33(23-24):1619-
- 1144 34.
- 1145 63. van der Lee R, Buljan M, Lang B, Weatheritt RJ, Daughdrill GW, Dunker AK, et al.
- 1146 Classification of intrinsically disordered regions and proteins. Chem Rev.
- 1147 2014;114(13):6589-631.
- 1148 64. Moesa HA, Wakabayashi S, Nakai K, Patil A. Chemical composition is maintained in
- poorly conserved intrinsically disordered regions and suggests a means for their
- classification. Mol Biosyst. 2012;8(12):3262-73.
- 1151 65. Mimori-Kiyosue Y, Shiina N, Tsukita S. Adenomatous polyposis coli (APC) protein
- moves along microtubules and concentrates at their growing ends in epithelial cells.
- 1153 J Cell Biol. 2000;148(3):505-18.
- 1154 66. Wiegand T, Hyman AA. Drops and fibers how biomolecular condensates and
- 1155 cytoskeletal filaments influence each other. Emerg Top Life Sci. 2020.
- 67. Simon C, Kusters R, Caorsi V, Allard A, Abou-Ghali M, Manzi J, et al. Actin dynamics
- drive cell-like membrane deformation. Nature Physics. 2019;15(6):602-9.
- 1158 68. Brouhard GJ, Rice LM. Microtubule dynamics: an interplay of biochemistry and
- mechanics. Nat Rev Mol Cell Biol. 2018;19(7):451-63.
- 69. Case LB, Ditlev JA, Rosen MK. Regulation of Transmembrane Signaling by Phase
- 1161 Separation. Annu Rev Biophys. 2019;48:465-94.
- 1162 70. Holehouse AS, Pappu RV. Functional Implications of Intracellular Phase Transitions.
- Biochemistry. 2018;57(17):2415-23.
- 1164 71. Banjade S, Rosen MK. Phase transitions of multivalent proteins can promote
- clustering of membrane receptors. Elife. 2014;3.
- 1166 72. Su X, Ditlev JA, Hui E, Xing W, Banjade S, Okrut J, et al. Phase separation of signaling
- molecules promotes T cell receptor signal transduction. Science.
- 1168 2016;352(6285):595-9.
- 1169 73. Case LB, Zhang X, Ditlev JA, Rosen MK. Stoichiometry controls activity of phase-
- separated clusters of actin signaling proteins. Science. 2019;363(6431):1093-7.
- 1171 74. McIntosh JR, O'Toole E, Morgan G, Austin J, Ulyanov E, Ataullakhanov F, et al.
- 1172 Microtubules grow by the addition of bent guanosine triphosphate tubulin to the
- tips of curved protofilaments. J Cell Biol. 2018;217(8):2691-708.
- 1174 75. Margolin G, Gregoretti IV, Cickovski TM, Li C, Shi W, Alber MS, et al. The mechanisms

- of microtubule catastrophe and rescue: implications from analysis of a dimer-scale computational model. Mol Biol Cell. 2012;23(4):642-56.
- 76. Gardner MK, Charlebois BD, Janosi IM, Howard J, Hunt AJ, Odde DJ. Rapid microtubule self-assembly kinetics. Cell. 2011;146(4):582-92.
- 1179 77. Hyman AA, Karsenti E. Morphogenetic properties of microtubules and mitotic spindle assembly. Cell. 1996;84(3):401-10.
- 78. Al-Bassam J, Chang F. Regulation of microtubule dynamics by TOG-domain proteins XMAP215/Dis1 and CLASP. Trends Cell Biol. 2011;21(10):604-14.
- 1183 79. Howard J, Hyman AA. Growth, fluctuation and switching at microtubule plus ends.
  1184 Nat Rev Mol Cell Biol. 2009;10(8):569-74.
- 80. Brouhard GJ, Stear JH, Noetzel TL, Al-Bassam J, Kinoshita K, Harrison SC, et al.
- 1186 XMAP215 is a processive microtubule polymerase. Cell. 2008;132(1):79-88.
- 1187 81. Dragestein KA, van Cappellen WA, van Haren J, Tsibidis GD, Akhmanova A, Knoch TA, 1188 et al. Dynamic behavior of GFP-CLIP-170 reveals fast protein turnover on 1189 microtubule plus ends. J Cell Biol. 2008;180(4):729-37.
- 1190 82. Trivedi P, Palomba F, Niedzialkowska E, Digman MA, Gratton E, Stukenberg PT. The 1191 inner centromere is a biomolecular condensate scaffolded by the chromosomal 1192 passenger complex. Nat Cell Biol. 2019;21(9):1127-37.
- 1193 83. Franck AD, Powers AF, Gestaut DR, Gonen T, Davis TN, Asbury CL. Tension applied 1194 through the Dam1 complex promotes microtubule elongation providing a direct 1195 mechanism for length control in mitosis. Nat Cell Biol. 2007;9(7):832-7.
- 84. Akiyoshi B, Sarangapani KK, Powers AF, Nelson CR, Reichow SL, Arellano-Santoyo H, et al. Tension directly stabilizes reconstituted kinetochore-microtubule attachments.

  Nature. 2010;468(7323):576-9.
- $\,$  1199  $\,$  85. Alberti S. Phase separation in biology. Curr Biol. 2017;27(20):R1097-R102.

1200

Fig 1

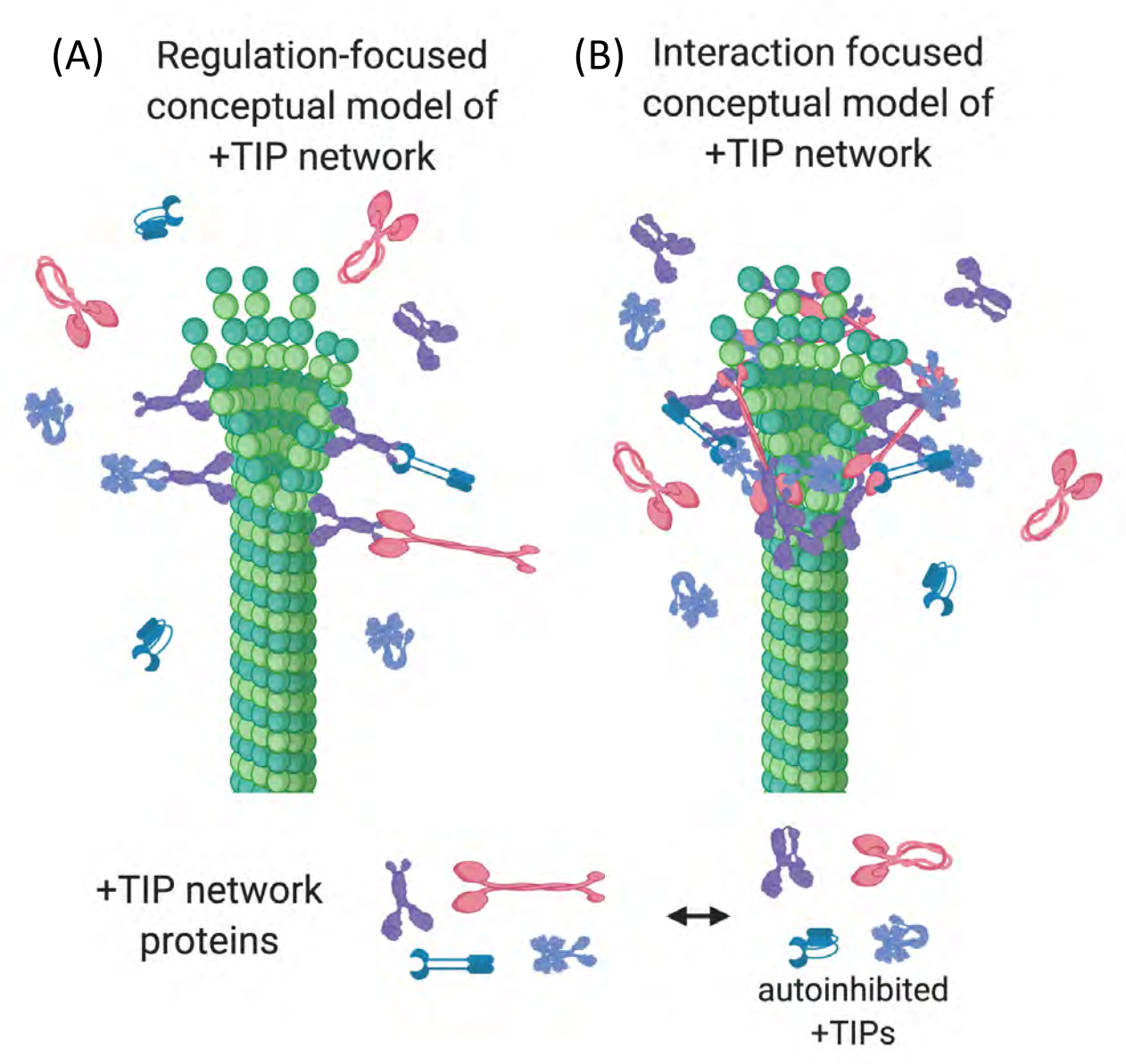


Fig 2

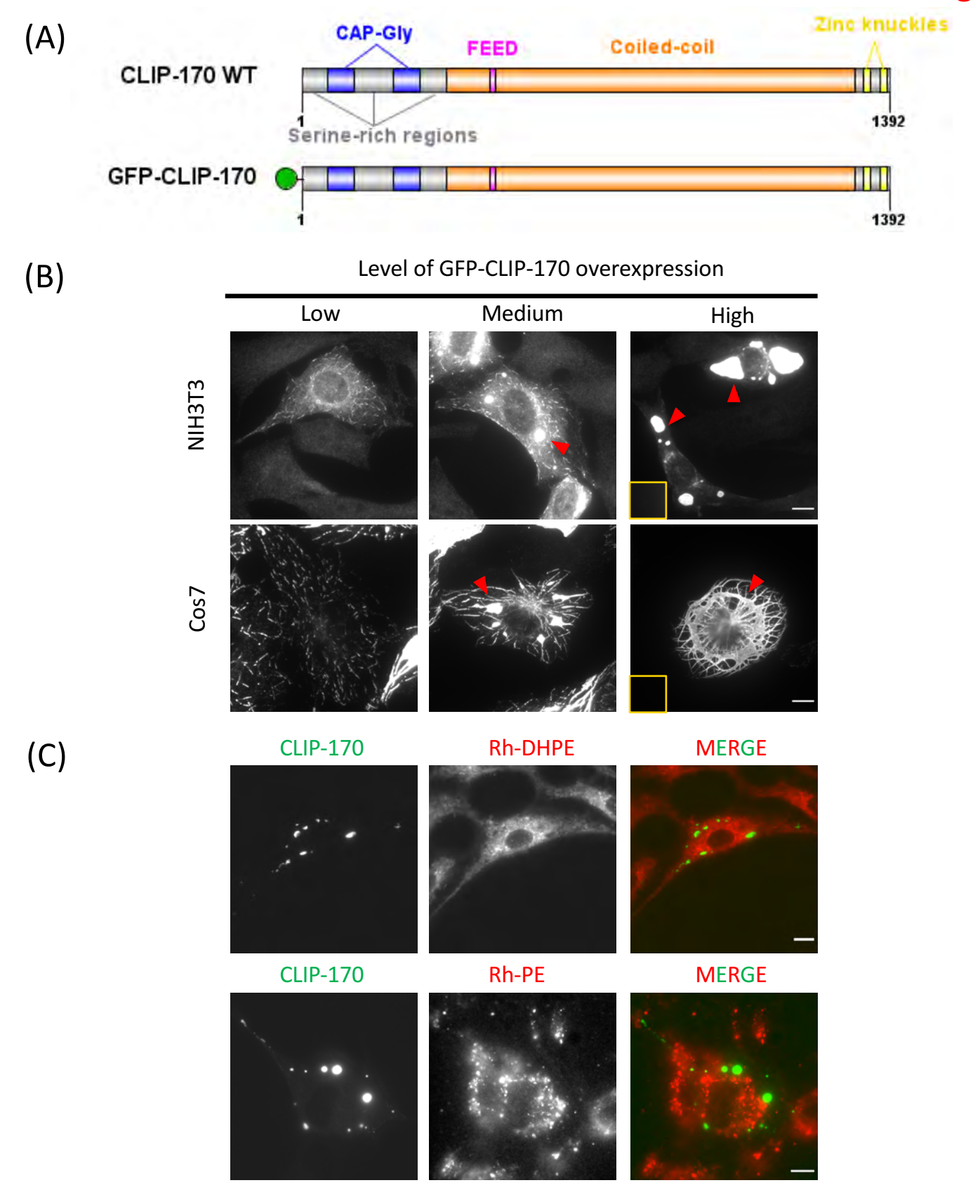
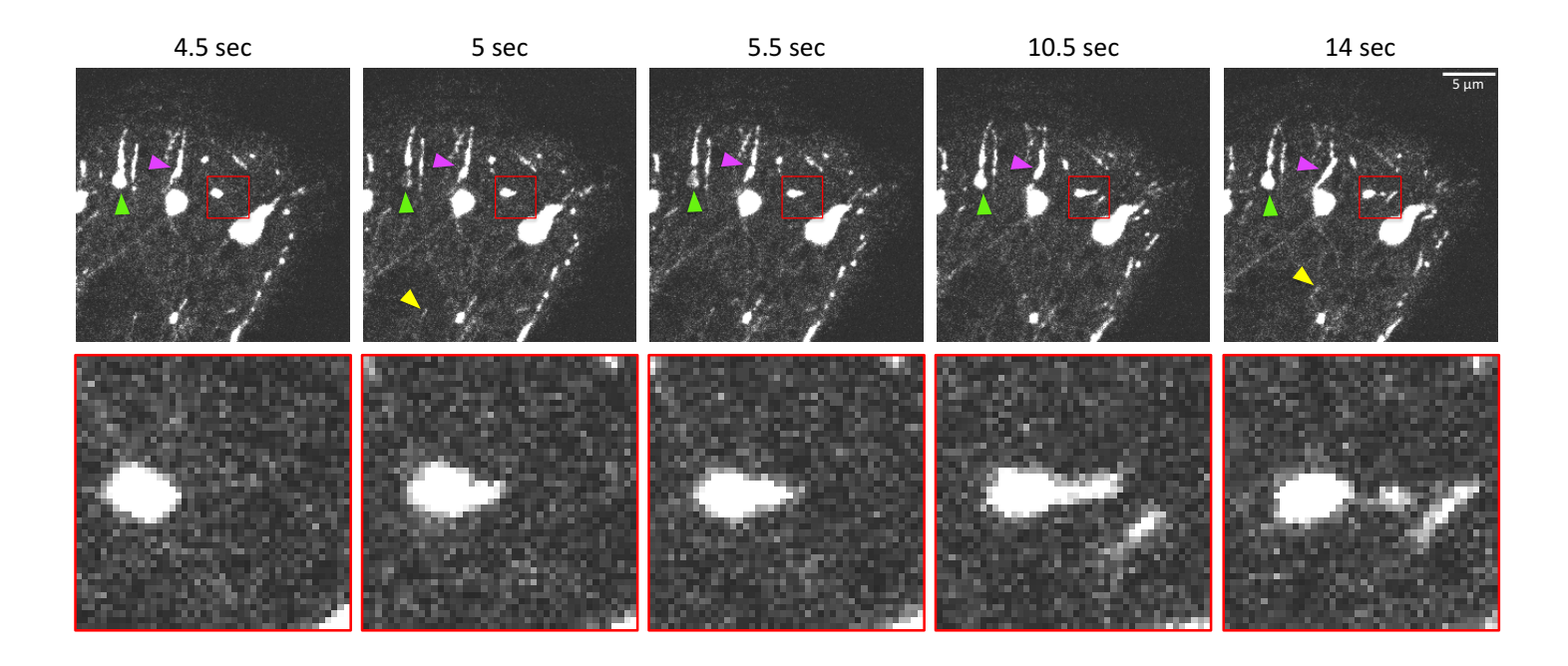
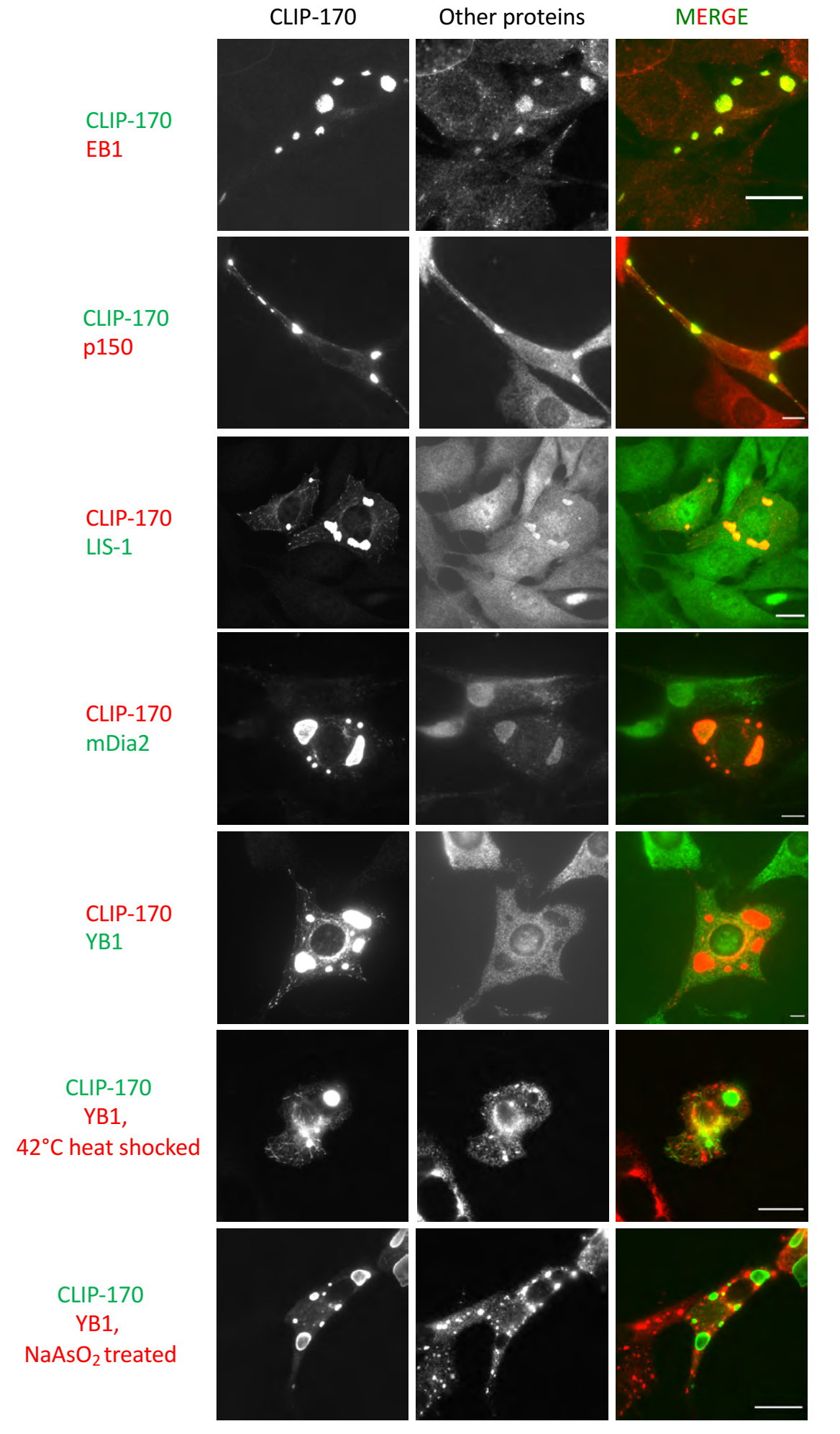
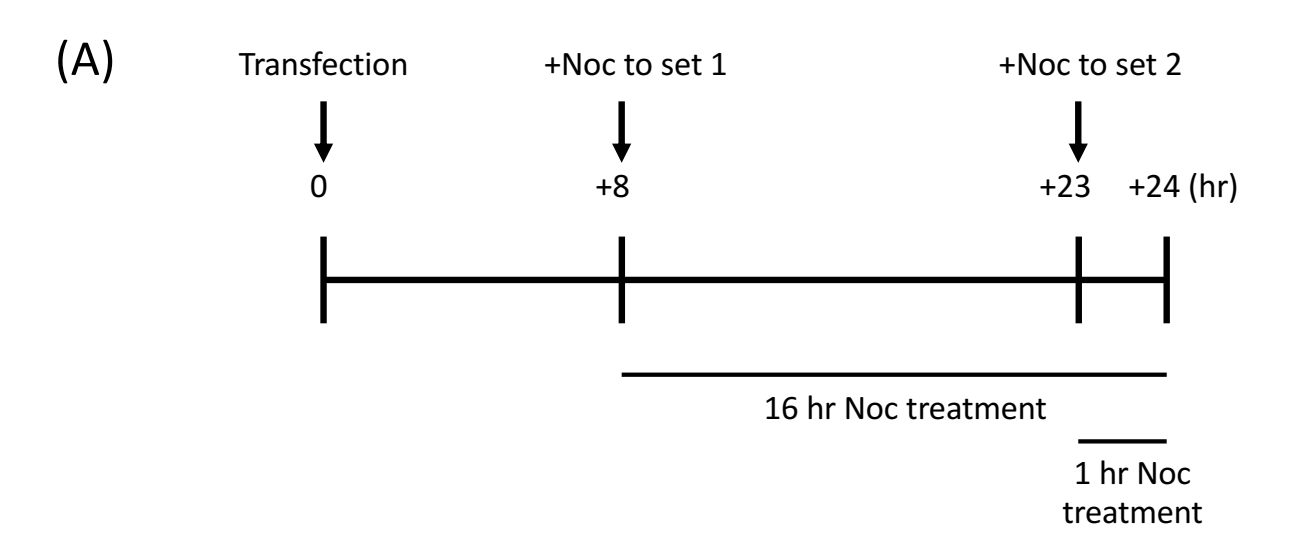
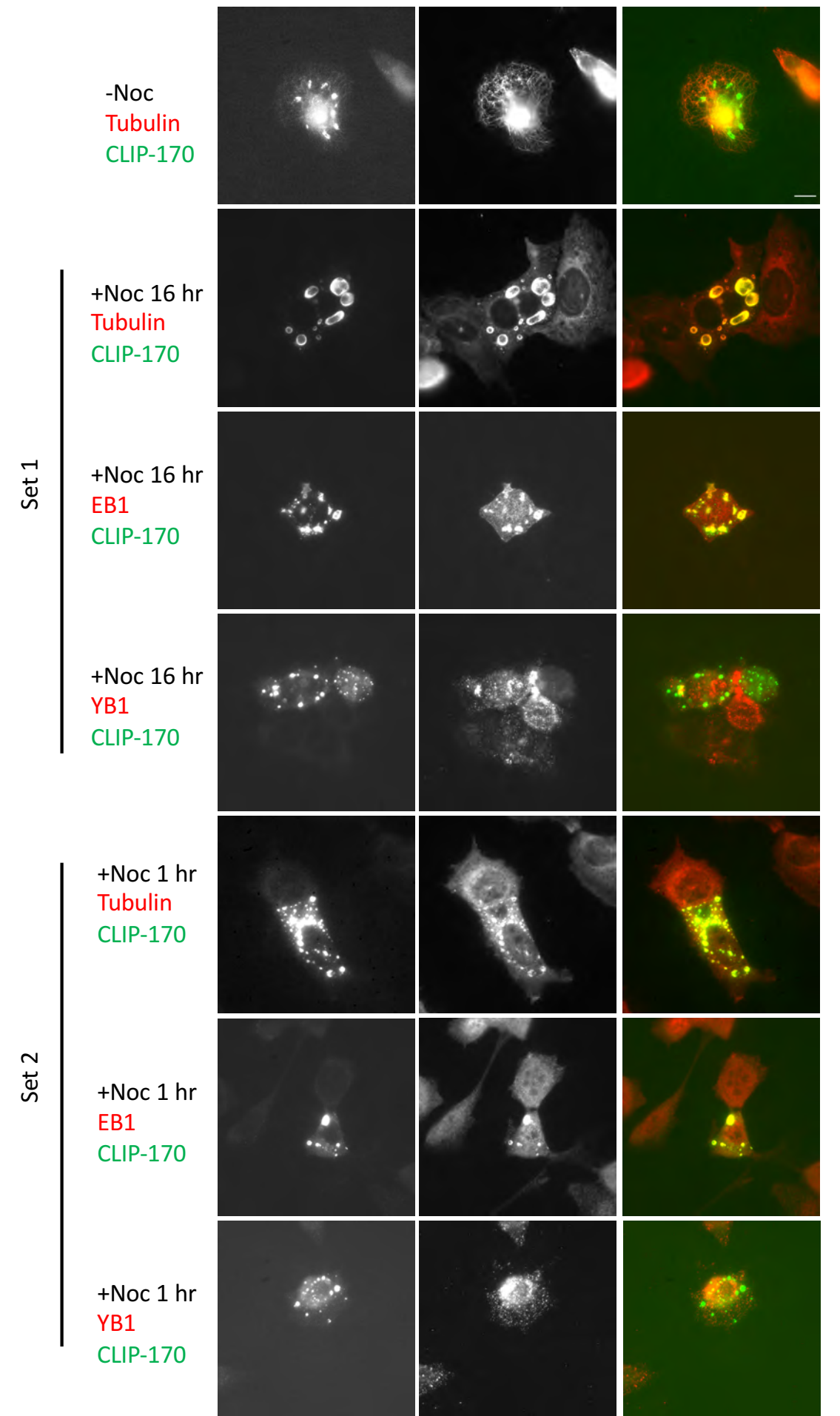


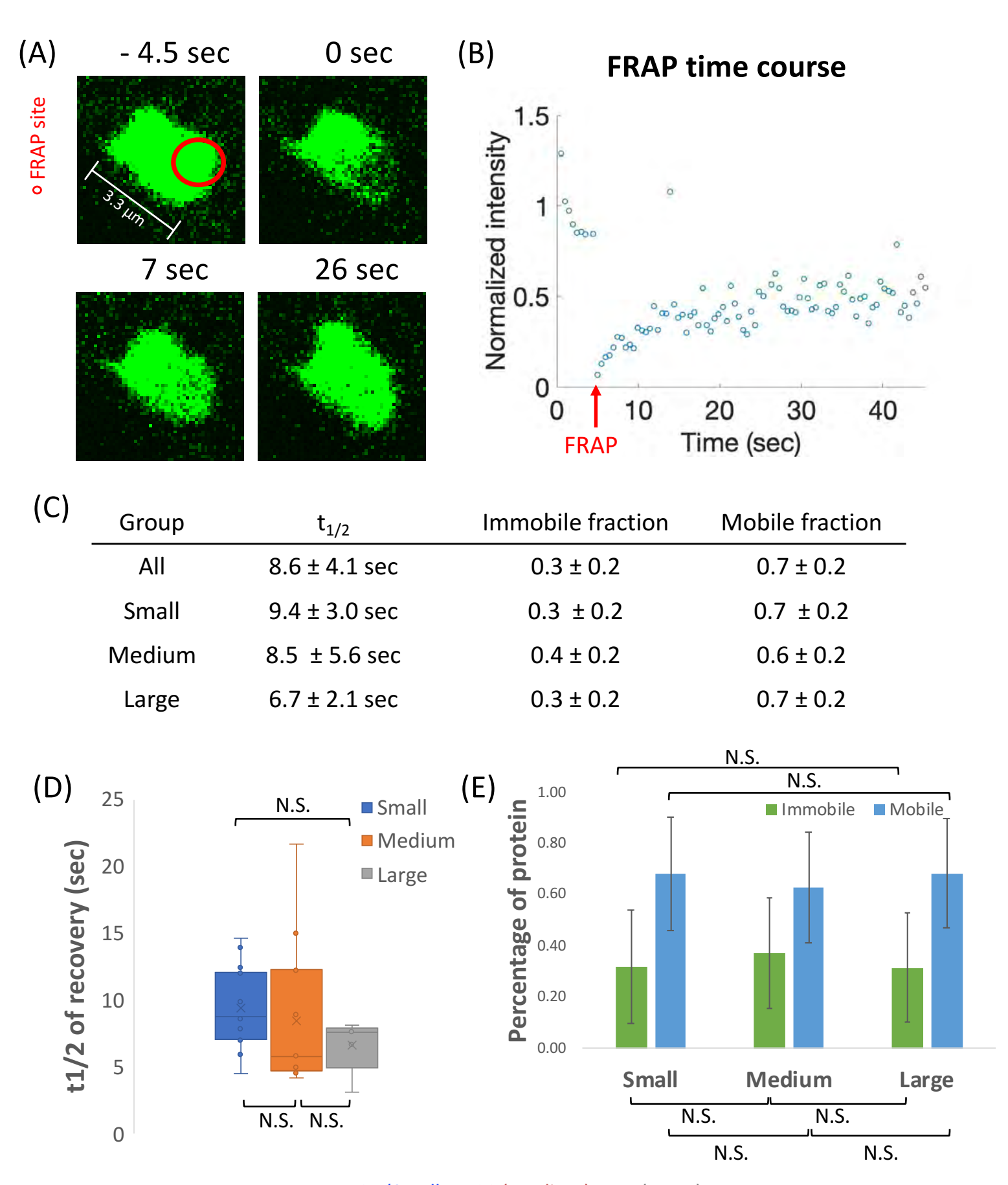
Fig 3











n=14 (Small; n=11 (Medium); n=5 (Large)

Fig 7 Zinc knuckles CAP-Gly Coiled-coil FEED 1392 Serine-rich regions coiled-coil (%) **Probability of** 0.5 0 200 400 1200 600 800 1000 Probability of Probability of IDRs (%) IDRs (%) 0.5

800

1000

1200

0 0

200

400

600

H. sapiens, CLIP-170 AAA35693.1 IDR% = 23.77%

M. musculus, CLIP1 NP\_062739.2 IDR% = 23.29% Per. Ident.: 89.66%

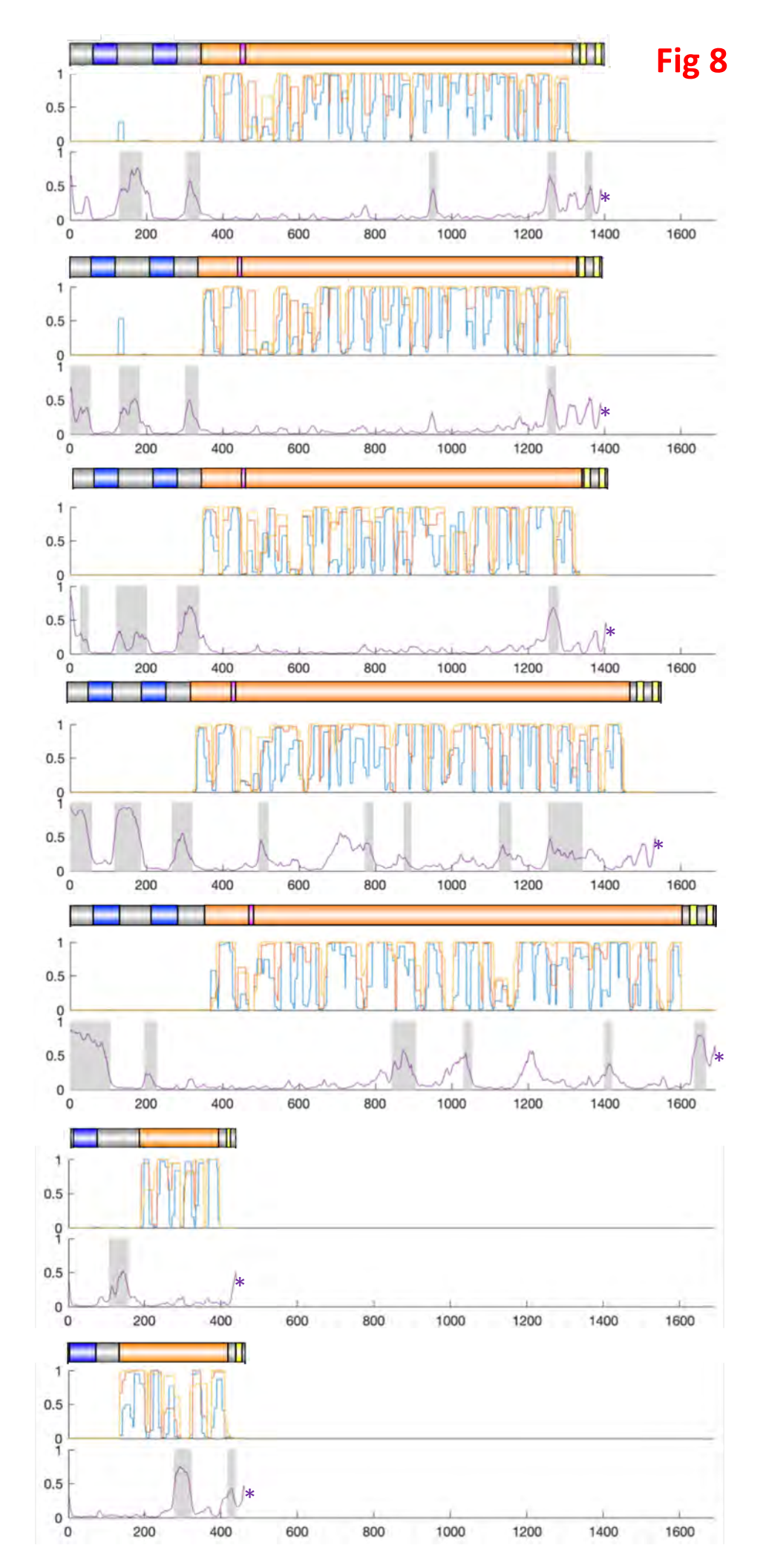
X. laevis, CLIP1 XP\_018118619.1 IDR% = 21.49% Per. Ident.: 60.30%

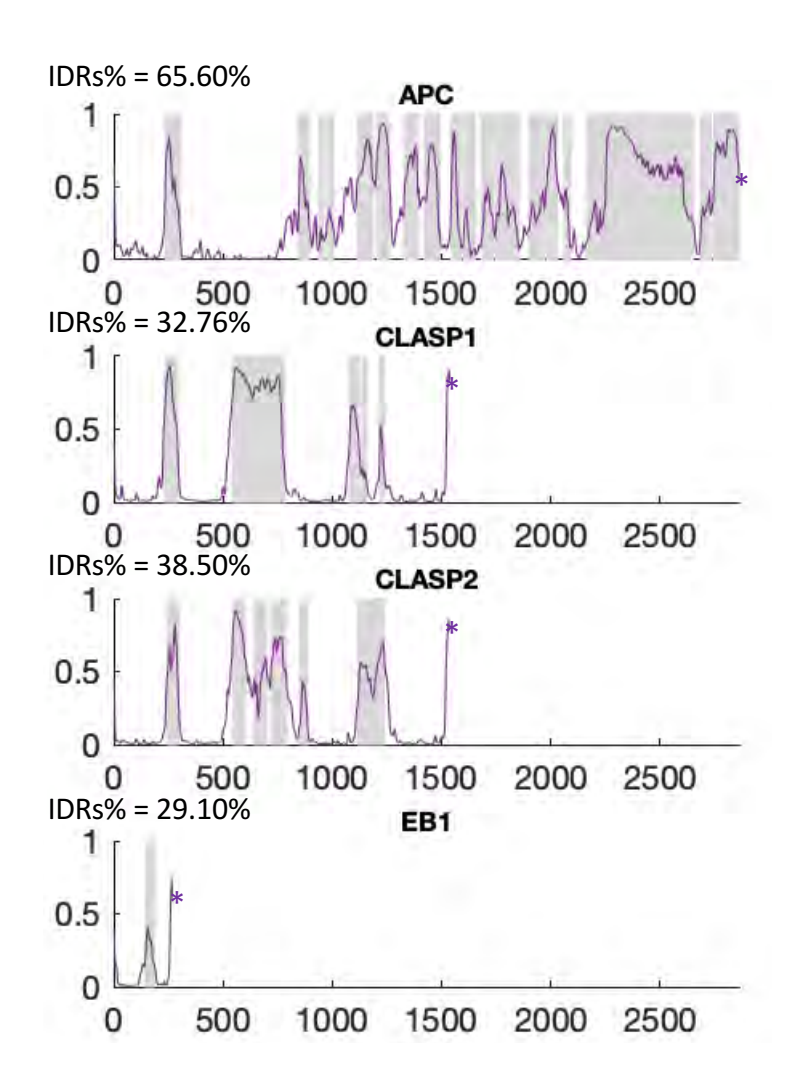
D. rerio, CLIP1 XP\_009300269.1 IDR% = 46.41% Per. Ident.: 48.14%

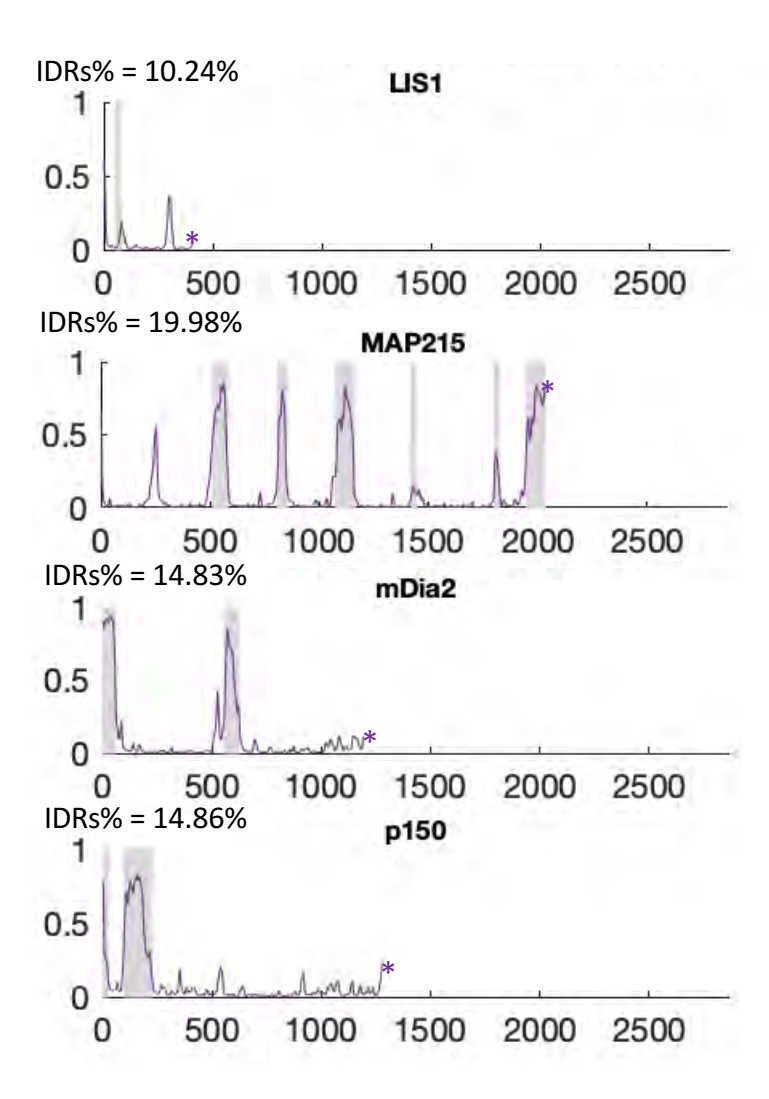
D. melanogaster, CLIP-190 NP\_609835.2 IDR% = 30.23% Per. Ident.: 33.39%

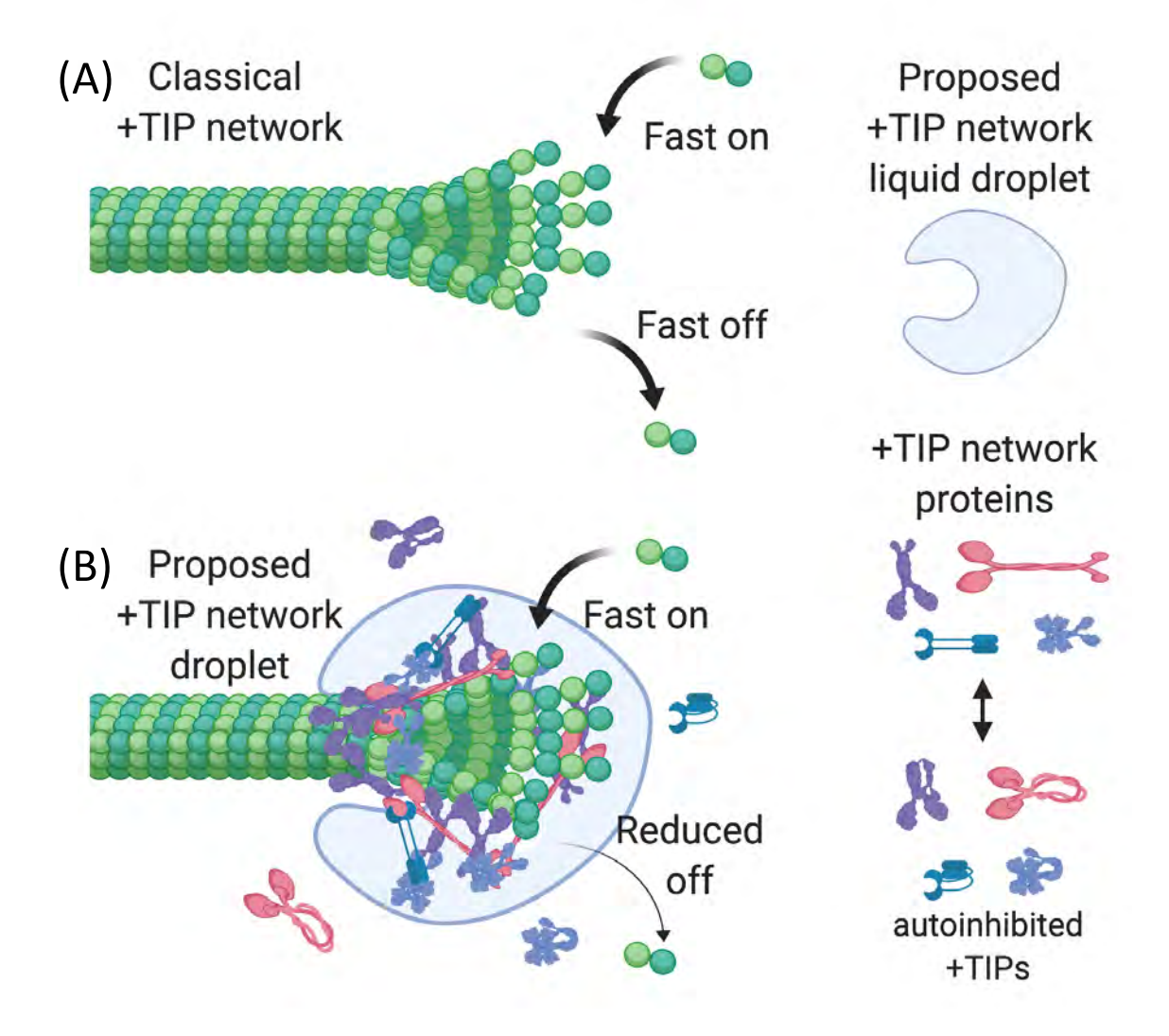
S. cerevisiae, Bik1p NP\_009901.1 IDR% = 17.95% Per. Ident.: 23.47%

S. pombe, Tip1 NP\_593613.1 IDR% = 27.98% Per. Ident.: 26.54%









# Supplement to the manuscript "Overexpression of the microtubule-binding protein CLIP-170 induces a +TIP network superstructure consistent with a biomolecular condensate"

## **Supplement Table of Contents**

<u>Figure/Tabl</u>	Cantion	Dago	
<u>e</u>	<u>Caption</u>	<u>Page</u>	
Movies	Legends for Movie 1-4	2	
S1 Table	Example of +TIP knock-out mutants from literature	3	
S1 Fig	A free C-terminal ETF motif is required for CLIP-170 to form patches	4	
S2 Fig	Membrane colocalization studies suggest that CLIP-170 patches are membraneless structures	5-6	
S3 Fig	CLIP-170 patches have selective properties	7	
S4 Fig	Staining of CLIP-170 patches and tubulin after PFA fixation	8	
S5 Fig	CLIP-170 forms patches at an early stage of transient transfection	9	
S6 Fig	Analysis of the size distribution of CLIP-170 condensates	10	
S7 Fig	The position of CLIP-170 IDRs is conserved from yeast to humans	11	
S8 Fig	Analysis of coiled-coil domains and IDRs of +TIP network proteins	12-13	
S9 Fig	Analysis of the position of coiled-coil domains and IDRs in EB1 across a range of organisms	14-15	
S10 Fig	Analysis of the position of coiled-coil domains and IDRs in MAP215 across a range of organisms	16-17	
S11 Fig	Analysis of the position of coiled-coil domains and IDRs in CLASPs across a range of organism	18-20	
References	References for the supplementary material	21-22	

Movie 1. Dynamic behavior of GFP-CLIP-170 in vivo when expressed at low levels. NIH3T3 cells were transiently transfected to express GFP-CLIP-170 for 24-27 hr, and the time-lapse images of 1 untransfected cell (number 0) and 4 transfected cells (numbers 1-4) were recorded by widefield microscopy. The numbers 1-4 correspond to the transfection level as assessed by the fluorescence intensity of the comets, with 1 and 4 indicating the lowest and highest levels of transfection respectively.

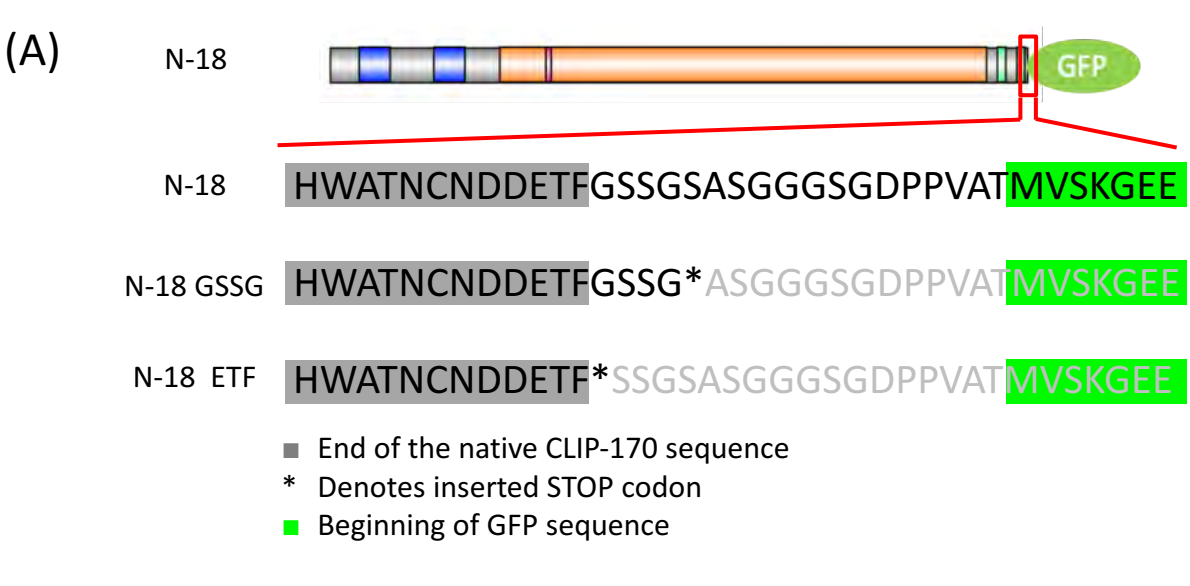
Movie 2. Micro-condensates appear in cells expressing medium-low levels of transfected GFP-CLIP-170. Time-lapse images of a NIH3T3 cell expressing a medium-low level of GFP-CLIP-170 were recorded by widefield microscopy after 24-27 hr of transient transfection. Arrows indicate examples of apparent micro-condensates. However, it is difficult to distinguish comets from condensates.

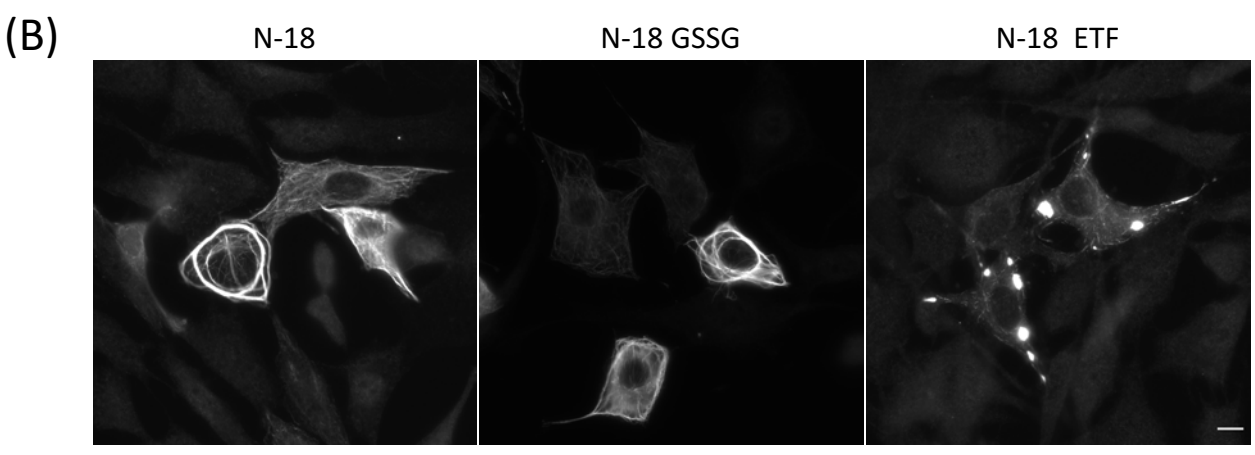
Movie 3. Dynamic behaviors of GFP-CLIP-170 patches in cells (this movie corresponds to Fig 3). NIH3T3 cells were transiently transfected with GFP-CLIP-170, and the behavior of GFP-CLIP-170 in cells was recorded by confocal microscopy after 24-27 hr of transfection. Red box: An example of an apparent elastic deformation of a patch, followed by fission. Arrows indicate examples of patch fusion (magenta) and a photobleached site (green).

**Movie 4. Dynamic behaviors of CLIP-170 patches in cells.** NIH3T3 cells were transiently transfected with GFP-CLIP-170 for 24-27 of transfection. Time-lapse images of a cell expressing small CLIP-170 patches were recorded by widefield microscopy. The top arrow shows an example of comets going through and deforming a CLIP-170 patch. The bottom arrow shows an example of apparent micro-condensates.

Table S1. Example of +TIP knock-out mutants from literature

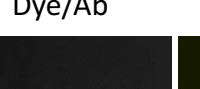
Protein (family), organism	Paralogs present	Viability	Other phenotypes	Reference(s)	
CLIP-170 (CLIP- 170), mice	CLIP-115	Viable	Male KO mice have abnormal sperm morphology.	(1, 2)	
CLIP-115 (CLIP- 170), mice	CLIP-170	Viable	KO mice develop Williams syndrome, including mild growth deficiency and other neuron development related symptoms.	(2, 3)	
CLIP-190 (CLIP- 170), fruit fly	No	Viable	Flies with null allele of <i>clip-190</i> have no obvious defects.	(4)	
BIK1 (CLIP-170), S. cerevisiae	No	Viable	Yeast with null-allele of <i>bik1</i> have a similar reproductive rate to wt, however, their nuclear positioning is abnormal.	(5-7)	
EB1 (EB), HeLa cells	EB2, EB3	Viable	Combined EB1/2/3 knock out HeLa cells can still go through mitosis but has some spindle abnormalities.	(8)	
DmEB1 (EB), fruit fly		Viable as larvae	Point mutation with reduced amount of DmEB1 is lethal due to failed eclosion. Surviving adults have abnormal wings and are flightless, which indicate neuromuscular defects.	(9)	
BIM1 (EB), S. cerevisiae	No	Viable	Synthetic lethality with bik1, num1, and bub3 deletion alleles.	(7, 10)	
AtEB1a (EB), Arabidopsis	AtEB1b, AtEB1c	Viable	Single or multiple-deletion of EB1 homologous genes have mild phenotypes (skewed root).	(11)	
Stu1 (CLASPs), S. cerevisiae	No	Inviable	Null mutant germinates and undergoes 1-2 cell divisions before cell division ceases.	(7, 12)	
CLASP (CLASPs),  Arabidopsis	No	Viable	Adult null mutant plants grow smaller, and have shorter inflorescences.	(13)	
Stu2 (MAP215), S. cerevisiae	No	Inviable	Null mutant germinates and undergoes 3-4 cell divisions before cell division ceases.	(14)	
Alp1 (MAP215), S. pombe	Dis1	Viable	$\Delta alp14$ mutant is viable but has abnormal mitotic progression. $\Delta alp14$ mutant is synthetic lethal with $dis1$ and $mad2$ .	(15)	
MACF1 (spectraplakin), mice	MACF2	Inviable	Mutant mice are not viable because of neuronal migration defects.	(2)	
MACF2 (spectraplakin), mice	MACF1	Viable	KO mice develop severe dystonia and sensory nerve degeneration.	(2, 16)	

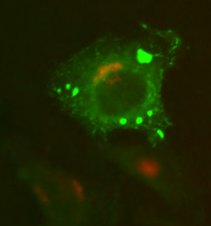




**S1 Fig.** A free C-terminal ETF motif is required for CLIP-170 to form patches. The CLIP-170 ETF motif mimics the tubulin E-hook and mediates both autoinhibitory and intramolecular interactions (17). (A) The protein sequences at the C-terminal ends of the CLIP-170 constructs in this experiment: N-18, N18 GSSG, and N-18 ETF. As shown here, N-18 has a C-terminal EGFP tag, N-18 GSSG has a short GSSG tag, and N-18 ETF has a native C-terminus (no tag). (B) NIH3T3 cells were transfected with N-18, N-18 GSSG, and N-18 ETF for 18 hr before methanol fixation. Cells were probed with a polyclonal antibody directed against the *Xenopus* CLIP-170 protein and imaged by widefield fluorescence microscopy. These images provide representative examples of the behaviors of these constructs and show that among these three N-18 constructs, only CLIP-170 with a free C-terminus has the ability to form patches. Scale bar: 10 μm. *Note:* The CLIP-170 isoform in the N-18 series is different from that used in the rest of the paper. More specifically, the N18 series corresponds to XP\_016875275.1, while the construct used elsewhere corresponds to AAA35693; these constructs differ by the insertion of 35 amino acids into XP\_016875275.1 after the FEED domain. However, we have not observed differences in the phenotypes exhibited by untagged constructs based on these two different splice isoforms.

CLIP-17

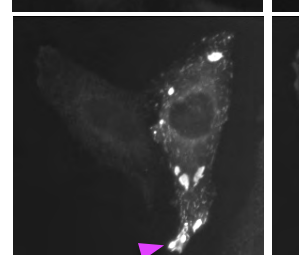


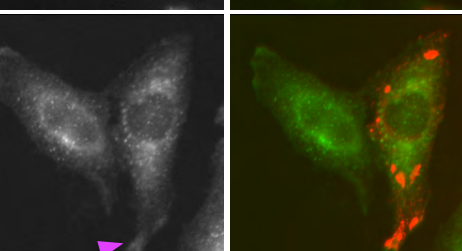


**MERGE** 

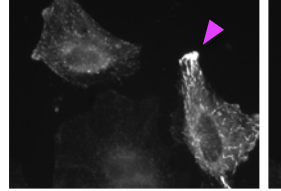
CLIP-170 EEA1

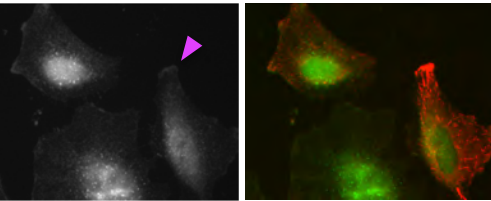
CLIP-170 GalT





CLIP-170 EEA1





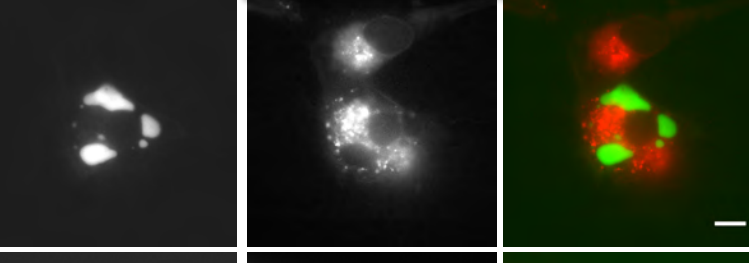
CLIP-170 Dil



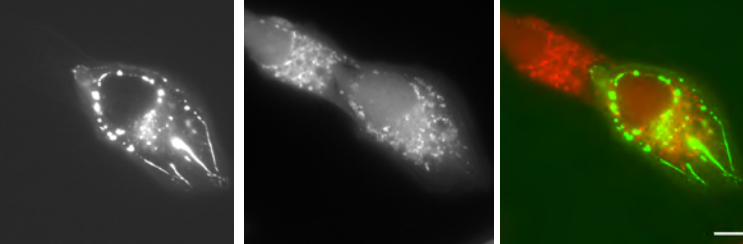
Zoom in to the yellow box: CLIP-170 Dil



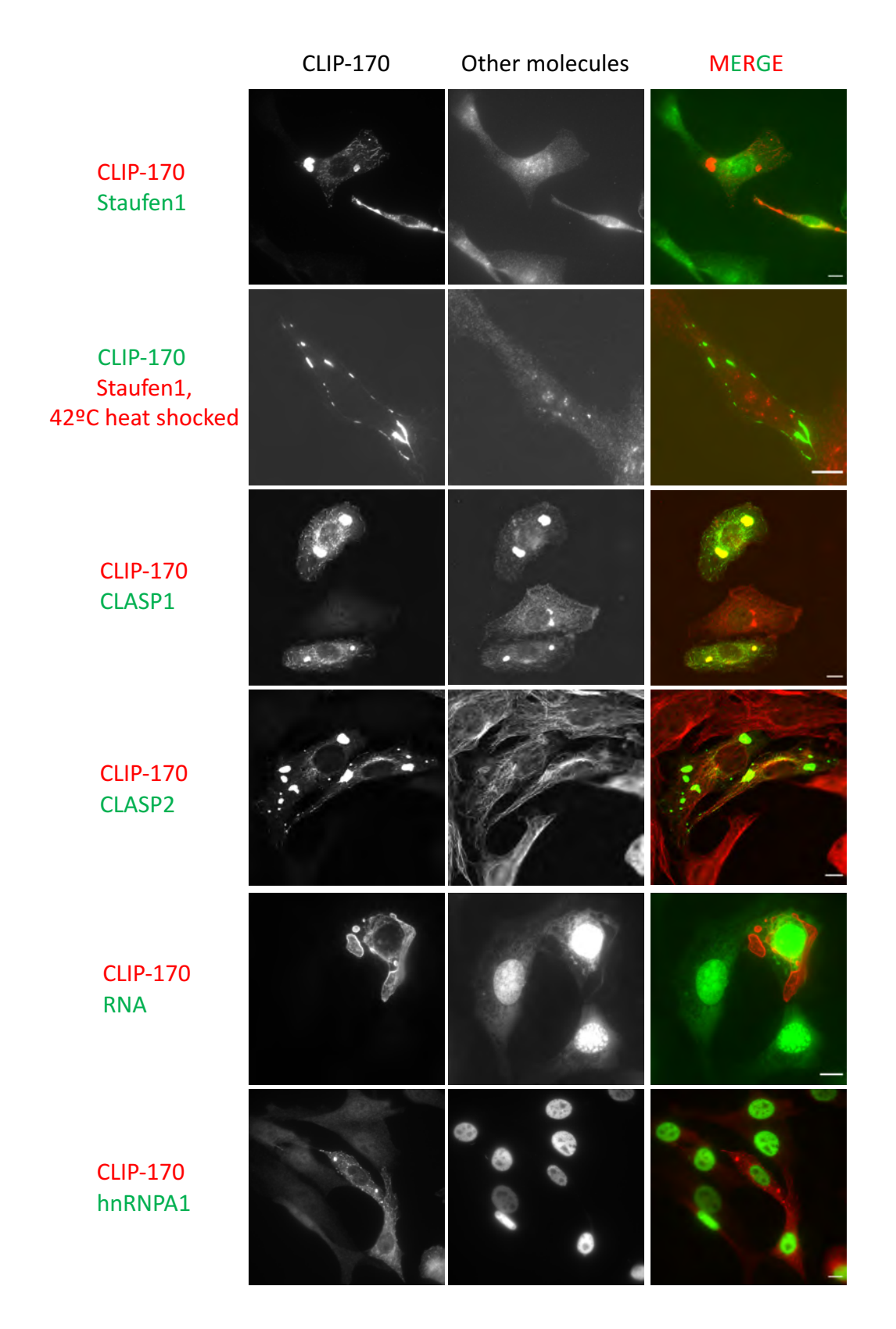
CLIP-170 Lysotracker



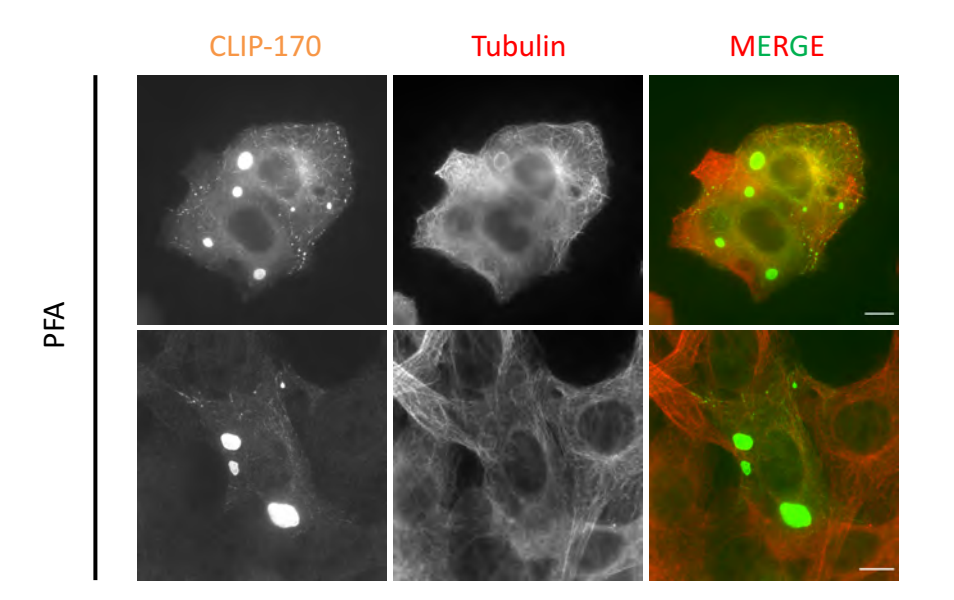
CLIP-170 Mitotracker



S2 Fig. Membrane colocalization studies suggest that CLIP-170 patches are membraneless structures. For the EEA1 and GalT experiments, HeLa cells were transfected with full-length CLIP-170 for 24-36 hr, then fixed with methanol before immunofluorescence imaging with antibodies as specified; the magenta arrows indicate partial colocalization between EEA1 and CLIP-170 patches. For the other experiments, NIH3T3 cells were transfected with GFP-CLIP-170 for 24-25 hr, stained by the specified lipid or organelle markers, and imaged live by widefield microscopy. Scale bar:  $10~\mu m$ .



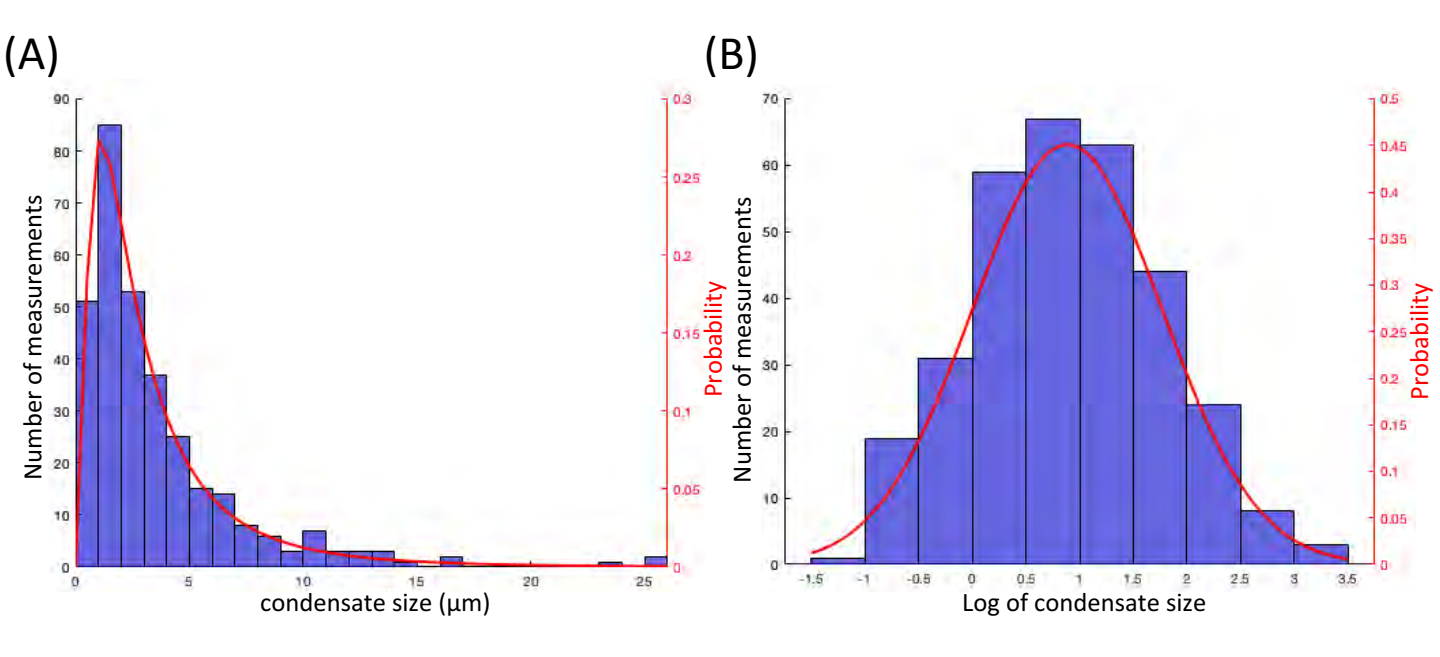
**S3 Fig. CLIP-170 patches have selective properties.** NIH3T3 cells were transfected with full-length CLIP-170 for 24 hr, fixed with PFA, probed with antibodies against molecules of interest (as indicated), and observed by widefield fluorescence microscopy. The contrast of each representative image in a given row is adjusted to the same levels. Scale bar:  $10 \, \mu m$ .



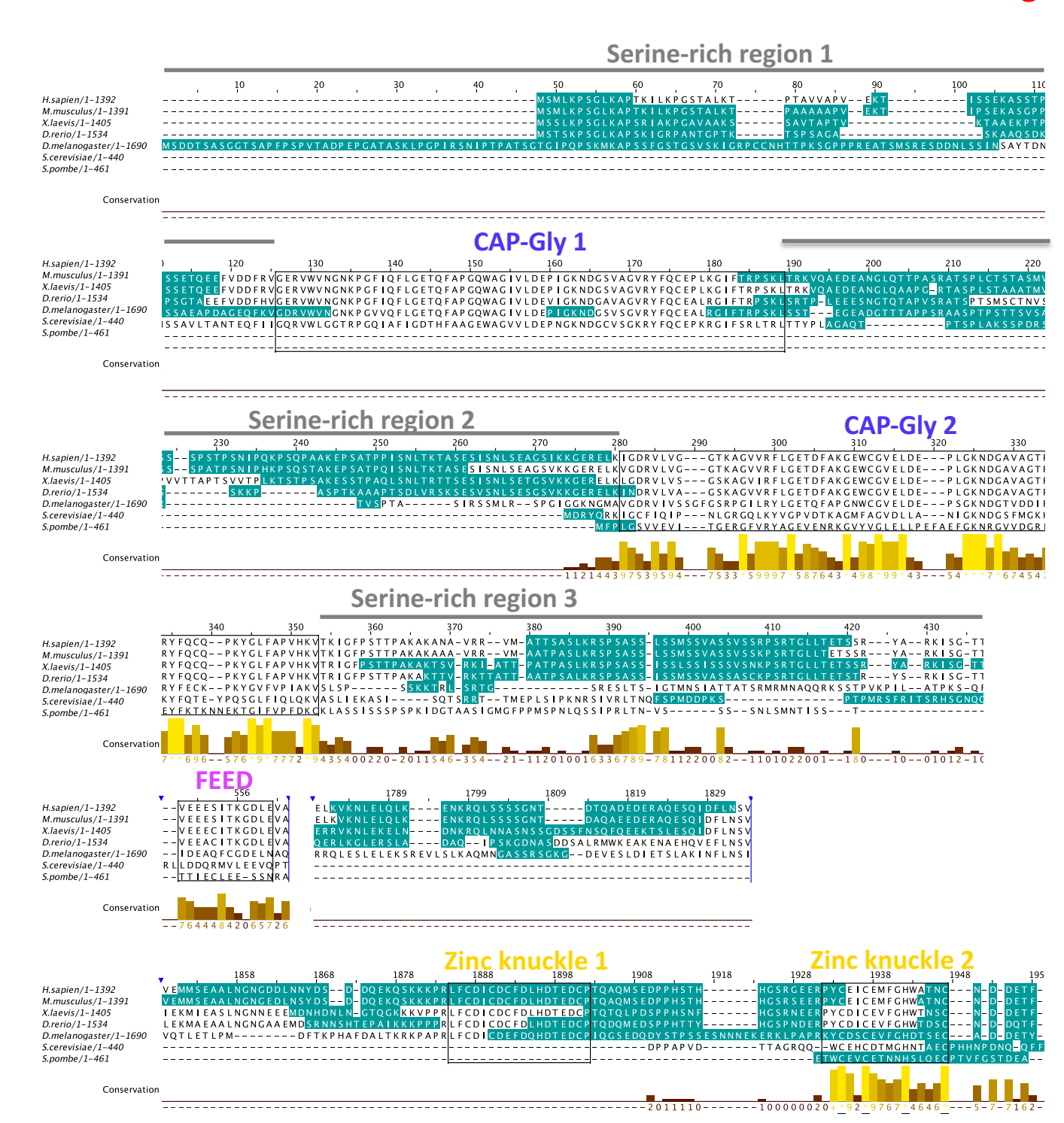
**S4 Fig. Staining of CLIP-170 patches and tubulin after PFA fixation.** NIH3T3 cells were transfected with full-length CLIP-170 for 24 hr, fixed with PFA, probed with antibodies against both CLIP-170 (rabbit antibodies against the *Xenopus* CLIP-170 protein) and tubulin (mouse monoclonal 1A2), and observed by widefield fluorescence microscopy. We observed that tubulin staining was variable in PFA. More specifically, sometimes the tubulin staining was limited to the outside of the patches (e.g., top row, middle panel, upper left patch), but in other cases it was difficult to discern the location of the patches by the tubulin staining alone (e.g., bottom panel). This behavior is in contrast to methanol fixation, where colocalization between microtubules and parts of the patches was clearer (Figure 5B, top row); in methanol-fixed cells, colocalization with tubulin in nocodazole-treated cells was prominent (Figure 5B). Scale bar:  $10 \, \mu m$ .

	8 hr transfection			24 hr transfection		
	Cell count	Percentage of total cells	Percentage of transfected cells	Cell count	Percentage of total cells	Percentage of transfected cells
Ends only	16	2.3%	64.0%	21	5.1%	65.6%
Ends & Patches	9	1.3%	36.0%	11	2.7%	34.4%
Bundles & Patches	0	0.0%	0.0%	0	0.0%	0.0%
Transfected cells	25	3.6%		32	7.7%	
Untransfected cells	677	96.4%		382	92.3%	
Total cell counts	702			414		

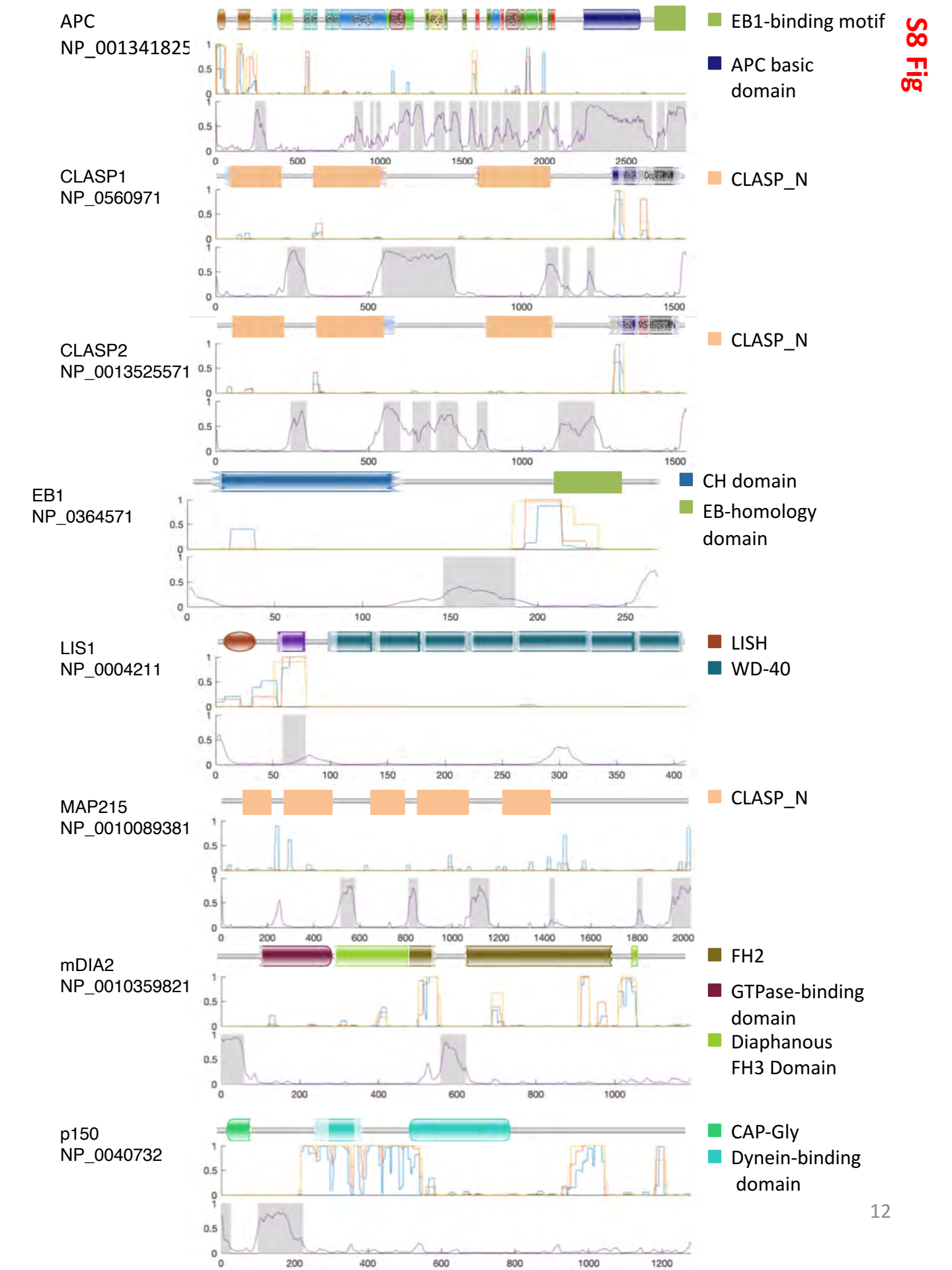
S5 Fig. CLIP-170 forms patches at an early stage of transient transfection. NIH3T3 cells were transfected with GFP-CLIP-170 and then fixed in methanol after 8 hr or 24 hr as indicated; the fixed cells were then observed by widefield fluorescence microscopy. Transfected cells and untransfected cells were counted, and the morphology of transfected cells was recorded and quantified. As expected, the observed transfection efficiency was higher after 24 hr of transfection. However, to our surprise, CLIP-170 patches were observed after both 8 hr and 24 hr of transfection, and the percentage of transfected cells with patches was similar in between the two time points. The observation that patches were observed at 8 hr indicates that CLIP-170 patches form soon after additional CLIP-170 is expressed.



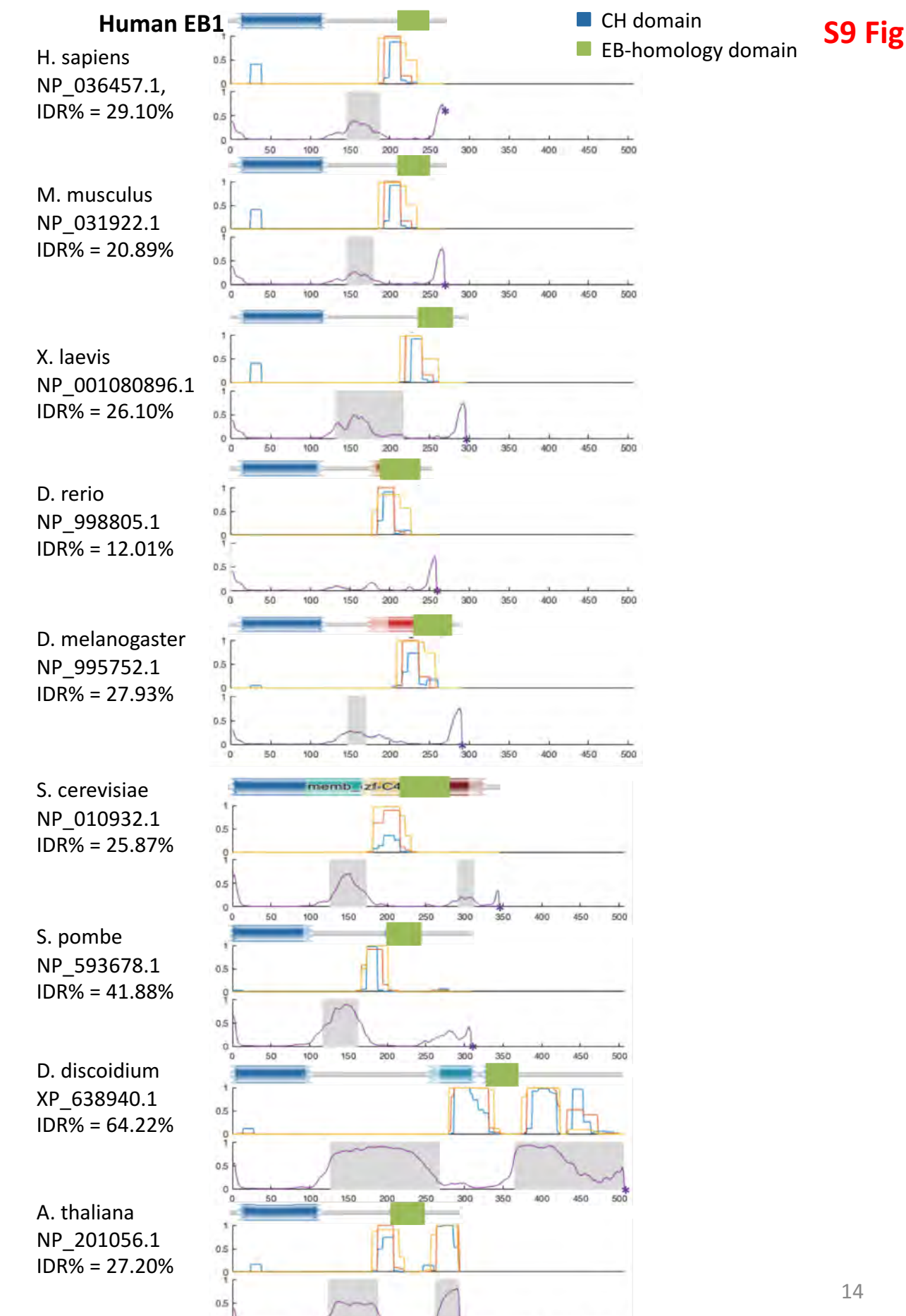
S6 Fig. Analysis of the size distribution of CLIP-170 condensates. To identify appropriate bin boundaries for separating condensates by size (Figs 6C-E), we used parametric distribution. (A) Histogram of condensate sizes as observed in 319 condensates from 100 fields of view. (B) Histogram of the log of condensate sizes from (A). To test whether the log-normal distribution was an appropriate parametric distribution to use for these data, we took the log of condensate sizes and fit it with a normal distribution (B), using Sturge's rule to determine the optimal bin size. These results support our decision to use a log-normal fit because the plot in (B) shows that our raw data in (A) is distributed in a log normal form. Image acquisition and quantification: NIH3T3 cells were transfected with GFP-CLIP-170. Cells were fixed with PFA after 24 hr of transfection, and 100 arbitrarily chosen fields of view were acquired using widefield fluorescence microscopy. For each condensate present in these images, we measured the widest width using Fiji, and this value was defined as the droplet size. A total of 319 condensates were measured. *Analysis of the* distribution of condensate sizes: The histogram of the condensate size distribution was plotted by the MATLAB "histogram" function. To determine the optimal bin size, we used the square-root model (a method commonly used for assessing skewed distributions). A Log-normal distribution was used to fit the histogram data. Finally, the "logniny" function was used to calculate the probability of condensate size falling within a certain range. We defined the smallest 50% of the condensates as small (0 - 2.4 µm), 50-75% as medium (2.4 - 4.4  $\mu$ m), and >75% as large ( $\geq$  4.4  $\mu$ m).



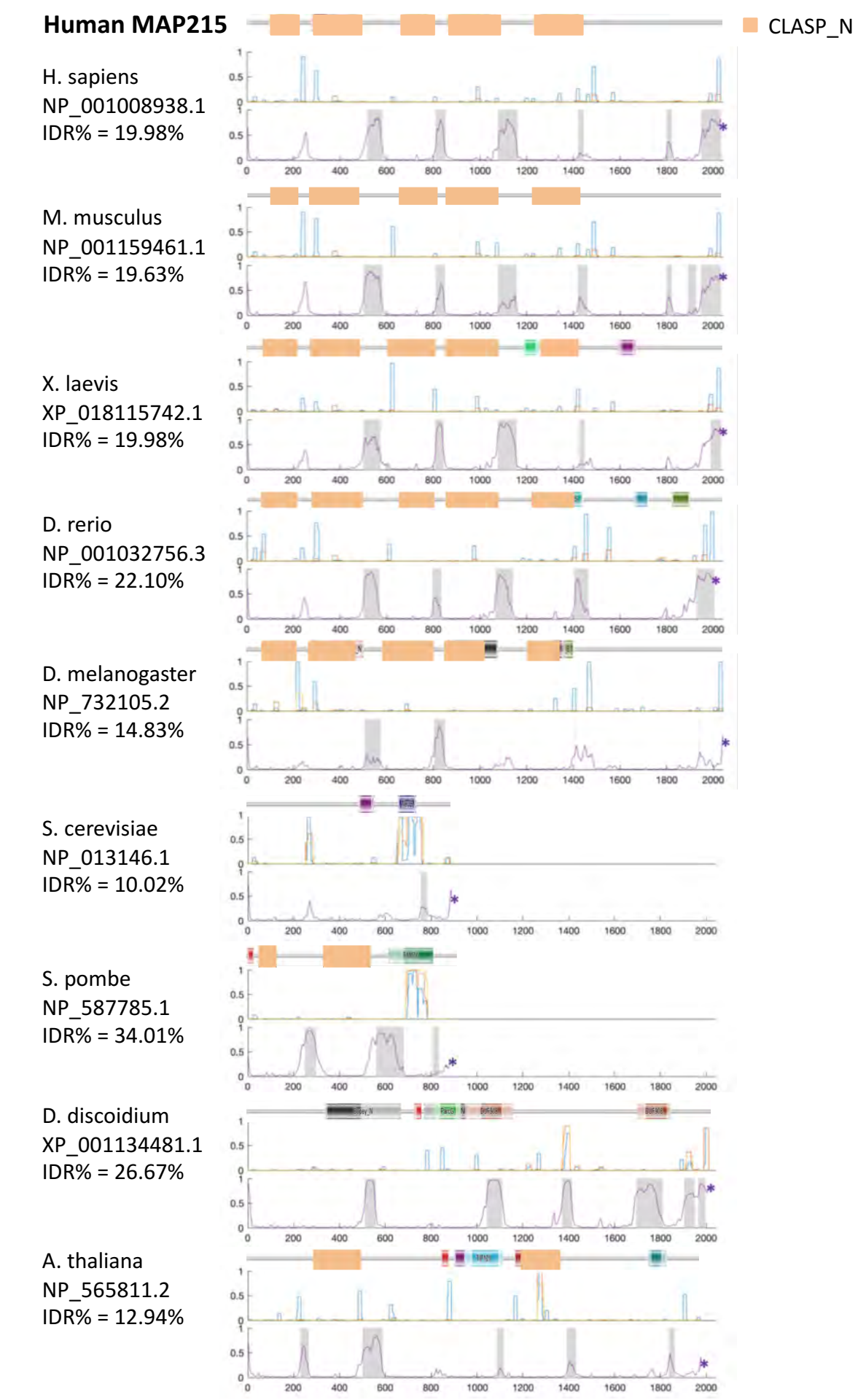
**S7 Fig. The position of CLIP-170 IDRs is conserved from yeast to humans.** Sequences here are the same as used in Fig 7. Cyan: disordered regions predicted by Espritz. Sequences are labeled with position in the alignment. Corresponding domain or motif structures were annotated above the aligned sequences. Annotations below were generated by Jalview and show the degree of conservation of the aligned columns.



**S8 Fig. Analysis of coiled-coil domains and IDRs of +TIP network proteins** (companion to Fig 9). For each +TIP network protein (accession number at left), the top image shows domain structures identified by Pfam (e-value < 0.1). For ease of visualization, we manually colored the most significant domains (as indicated on the right), while minor domains are shown as plotted by Pfam. Note that a few recognized domain structures were not predicted with the e-value we selected, meaning that the absence of a domain in this figure should not necessarily be interpreted as absence of the domain in the protein. The middle image represents the probability of coiled-coil region as predicted by COILS with three different windows (7AA, blue; 14 AA, orange; 21 AA yellow). In the bottom image, the purple line shows the probability of IDRs predicted by Espritz, and the shaded area indicates the IDRs as predicted by MobiDB-lite. For both COILS and Espritz analyses, 1 indicates 100% likelihood.

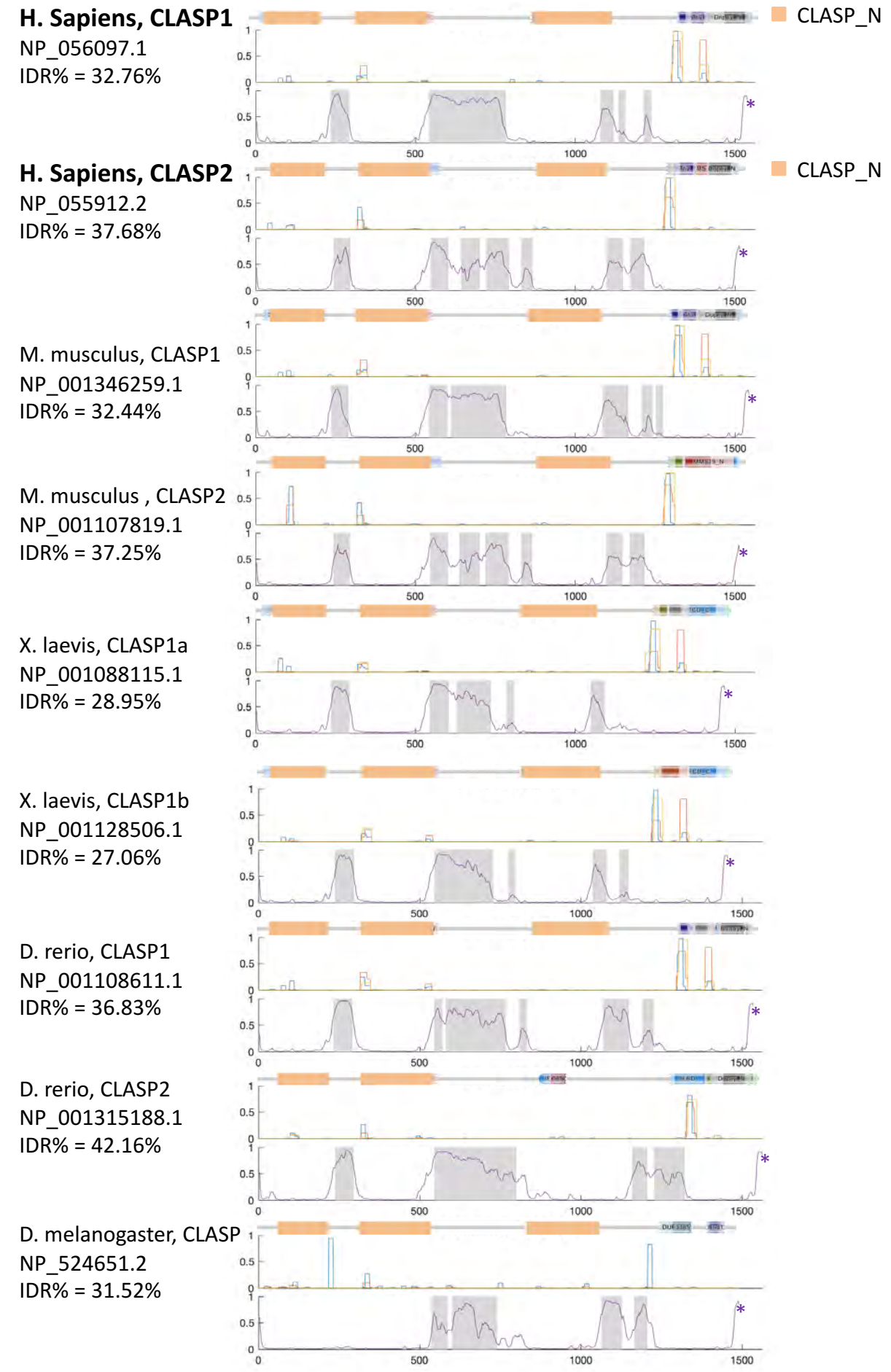


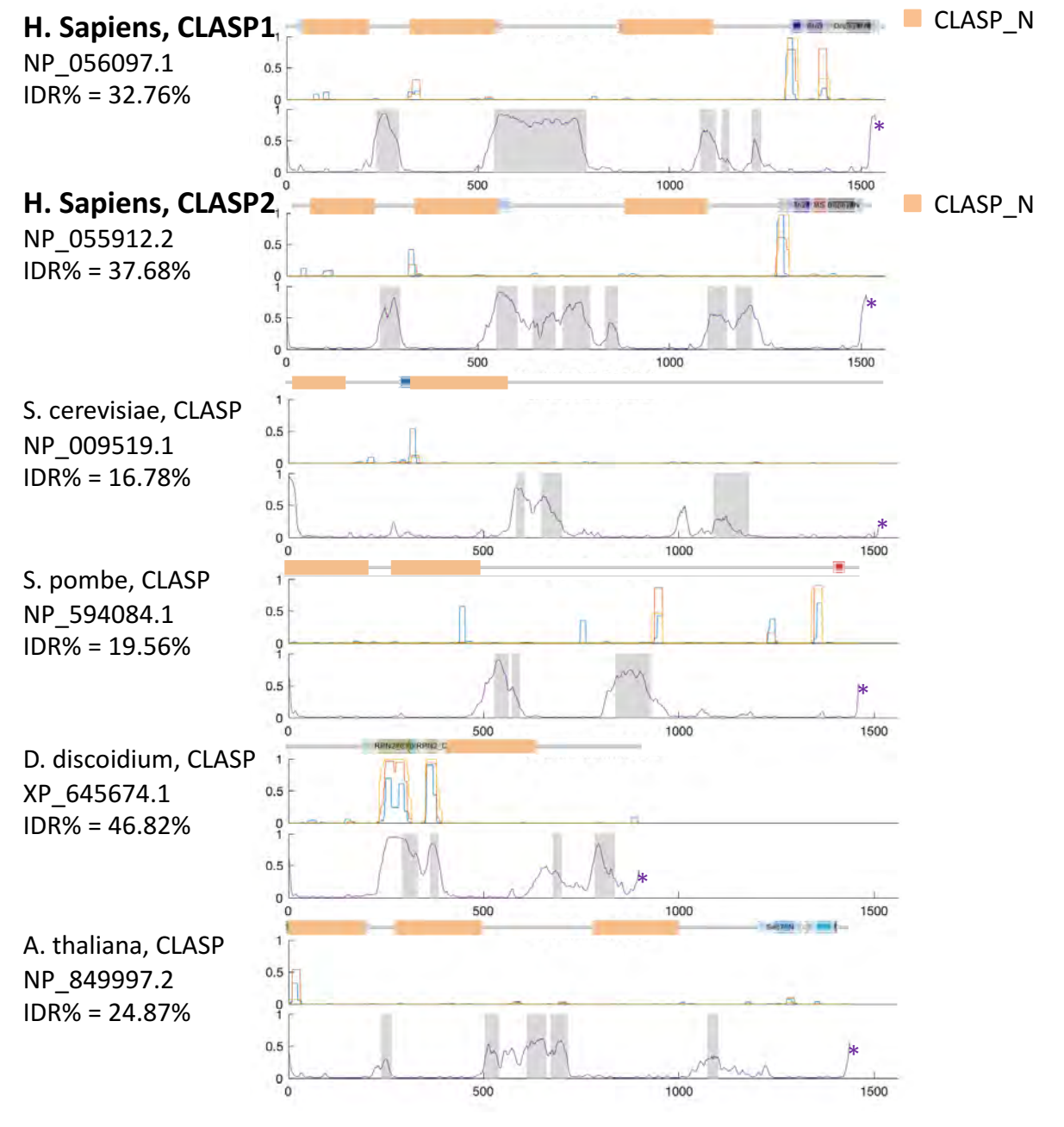
S9 Fig. Analysis of the position of coiled-coil domains and IDRs in EB1 across a range of organisms. For each EB1 protein (one chosen per species, accession number at left), the top image shows the domain structures identified by Pfam (e-value < 0.1). For ease of visualization, we manually colored the most significant domains (as indicated on the right), while minor domains are shown as plotted by Pfam. Note that a few recognized domain structures were not predicted with the e-value we selected, meaning that the absence of a domain in this figure should not necessarily be interpreted as absence of the domain in the protein. The middle image represents the probability of coiled-coil region as predicted by COILS with three different windows (7AA, blue; 14 AA, orange; 21 AA yellow). In the bottom image, the purple line shows the probability of IDRs predicted by Espritz, and the shaded area indicates the IDRs as predicted by MobiDB-lite. For both COILS and Espritz analyses, 1 indicates 100% likelihood. \* indicates the end of the sequence.



#### S10 Fig. Analysis of the position of coiled-coil domains and IDRs in MAP215 across a range of organisms.

For each MAP215 protein (one chosen per species, accession number at left), the top image shows the domain structures identified by Pfam (e-value < 0.1). For ease of visualization, we manually colored the most significant domains (as indicated on the right), while minor domains are shown as plotted by Pfam. Note that a few recognized domain structures were not predicted with the e-value we selected, meaning that the absence of a domain in this figure should not necessarily be interpreted as absence of the domain in the protein. The middle image represents the probability of coiled-coil region as predicted by COILS with three different windows (7AA, blue; 14 AA, orange; 21 AA yellow). In the bottom image, the purple line shows the probability of IDRs predicted by Espritz, and the shaded area indicates the IDRs as predicted by MobiDB-lite. For both COILS and Espritz analyses, 1 indicates 100% likelihood. \* indicates the end of the sequence.





#### S11 Fig. Analysis of the position of coiled-coil domains and IDRs in CLASPs across a range of organisms.

For each CLASP protein (one chosen per species, accession number at left), the top image shows the domain structures identified by Pfam (e-value < 0.1). For ease of visualization, we manually colored the most significant domains (as indicated on the right), while minor domains are shown as plotted by Pfam. Note that a few recognized domain structures were not predicted with the e-value we selected, meaning that the absence of a domain in this figure should not necessarily be interpreted as absence of the domain in the protein. The middle image represents the probability of coiled-coil region as predicted by COILS with three different windows (7AA, blue; 14 AA, orange; 21 AA yellow). In the bottom image, the purple line shows the probability of IDRs predicted by Espritz, and the shaded area indicates the IDRs as predicted by MobiDB-lite. For both COILS and Espritz analyses, 1 indicates 100% likelihood. \* indicates the end of the sequence.

### **Reference:**

- Akhmanova A, Mausset-Bonnefont AL, van Cappellen W, Keijzer N, Hoogenraad CC, Stepanova T, et al. The microtubule plus-end-tracking protein CLIP-170 associates with the spermatid manchette and is essential for spermatogenesis. Genes Dev. 2005;19(20):2501-15.
- 2. van de Willige D, Hoogenraad CC, Akhmanova A. Microtubule plus-end tracking proteins in neuronal development. Cell Mol Life Sci. 2016;73(10):2053-77.
- 3. Hoogenraad CC, Koekkoek B, Akhmanova A, Krugers H, Dortland B, Miedema M, et al. Targeted mutation of Cyln2 in the Williams syndrome critical region links CLIP-115 haploinsufficiency to neurodevelopmental abnormalities in mice. Nat Genet. 2002;32(1):116-27.
- 4. Dix CI, Soundararajan HC, Dzhindzhev NS, Begum F, Suter B, Ohkura H, et al. Lissencephaly-1 promotes the recruitment of dynein and dynactin to transported mRNAs. J Cell Biol. 2013;202(3):479-94.
- 5. Geiser JR, Schott EJ, Kingsbury TJ, Cole NB, Totis LJ, Bhattacharyya G, et al. Saccharomyces cerevisiae genes required in the absence of the CIN8-encoded spindle motor act in functionally diverse mitotic pathways. Mol Biol Cell. 1997;8(6):1035-50.
- 6. Berlin V, Styles CA, Fink GR. BIK1, a protein required for microtubule function during mating and mitosis in *Saccharomyces cerevisiae*, colocalizes with tubulin. J Cell Biol. 1990;111(6 Pt 1):2573-86.
- 7. Giaever G, Chu AM, Ni L, Connelly C, Riles L, Veronneau S, et al. Functional profiling of the Saccharomyces cerevisiae genome. Nature. 2002;418(6896):387-91.
- 8. Yang C, Wu J, de Heus C, Grigoriev I, Liv N, Yao Y, et al. EB1 and EB3 regulate microtubule minus end organization and Golgi morphology. J Cell Biol. 2017;216(10):3179-98.
- 9. Elliott SL, Cullen CF, Wrobel N, Kernan MJ, Ohkura H. EB1 is essential during *Drosophila* development and plays a crucial role in the integrity of chordotonal mechanosensory organs. Mol Biol Cell. 2005;16(2):891-901.
- 10. Schwartz K, Richards K, Botstein D. BIM1 encodes a microtubule-binding protein in yeast. Mol Biol Cell. 1997;8(12):2677-91.
- 11. Bisgrove SR, Lee YR, Liu B, Peters NT, Kropf DL. The microtubule plus-end binding protein EB1 functions in root responses to touch and gravity signals in *Arabidopsis*. Plant Cell. 2008;20(2):396-410.
- 12. Pasqualone D, Huffaker TC. STU1, a suppressor of a beta-tubulin mutation, encodes a novel and essential component of the yeast mitotic spindle. J Cell Biol. 1994;127(6 Pt 2):1973-84.
- 13. Kirik V, Herrmann U, Parupalli C, Sedbrook JC, Ehrhardt DW, Hulskamp M. CLASP localizes in two discrete patterns on cortical microtubules and is required for cell morphogenesis and cell division in *Arabidopsis*. J Cell Sci. 2007;120(Pt 24):4416-25.
- 14. Wang PJ, Huffaker TC. Stu2p: A microtubule-binding protein that is an essential component of the yeast spindle pole body. J Cell Biol. 1997;139(5):1271-80.
- 15. Garcia MA, Vardy L, Koonrugsa N, Toda T. Fission yeast ch-TOG/XMAP215 homologue Alp14 connects mitotic spindles with the kinetochore and is a component of the Mad2-dependent spindle checkpoint. EMBO J. 2001;20(13):3389-401.

- 16. Guo L, Degenstein L, Dowling J, Yu QC, Wollmann R, Perman B, et al. Gene targeting of BPAG1: abnormalities in mechanical strength and cell migration in stratified epithelia and neurologic degeneration. Cell. 1995;81(2):233-43.
- 17. Chen Y, Wang P, Slep KC. Mapping multivalency in the CLIP-170-EB1 microtubule plus-end complex. J Biol Chem. 2019;294(3):918-31.